

Unclassified Report
Nat.Lab. Unclassified Report 034/96

Comparison of Mextram and the Vbic95 bipolar transistor model

Author(s): W.J. Kloosterman

© *Philips Electronics N.V. 1996*
All rights are reserved. Reproduction in whole or in part is prohibited without the written consent of the copyright owner.

Unclassified Report: 034/96

Title: Comparison of Mextram and the Vbic95 bipolar transistor model

Author(s): W.J. Kloosterman

Part of project:

Customer:

Keywords: Mextram; Vbic95; compact models;

Abstract: Recently a new bipolar transistor model called Vbic95 is introduced to replace the aging standard Spice Gummel Poon model. In this report the Vbic95 release 1.1.4 is investigated and compared with the Philips bipolar transistor model Mextram release 503.2 . Also the conversion of Mextram model parameters to Vbic95 parameters is worked out.

Conclusions: The main improvement of the Vbic95 model over the SGP model are the implicit modelling of the parasitic PNP transistor, bias dependent output conductance, modelling of the epilayer resistance (base push-out), avalanche multiplication and the extensive temperature mapping. The Mextram and Vbic95 bipolar transistor models are comparable for low and medium collector current densities and frequencies.

The main deficiency of the Vbic95 model is the description of the velocity saturated behavior of the current through the collector epilayer in combination with base push-out. Monotony of the output conductance and cut-off frequency is not guaranteed when an epilayer resistance is present. Therefore the Vbic95 model is not able to describe accurately the degradation of gain, output conductance and cut-off frequency at high current densities.

Parameter conversion from Mextram to Vbic95 can easily be done for the depletion capacitances and DC parameters related to low and medium current levels. The conversion of the high bias related parameters is risky especially when the epilayer parameters are dominant. Then best case DC and AC parameters can only be obtained via parameter extraction.

Contents

| | | |
|-----------|---|-----------|
| 1 | Introduction | 1 |
| 2 | Electrical equivalent network | 1 |
| 3 | Depletion capacitances | 4 |
| 4 | Early voltages | 6 |
| 5 | Forward current gain | 10 |
| 5.1 | Collector current | 10 |
| 5.2 | Forward base current | 12 |
| 6 | Reverse current gain | 14 |
| 6.1 | Emitter current of the reverse Gummel plot. | 14 |
| 6.2 | Substrate current. | 16 |
| 6.3 | Reverse base current. | 18 |
| 7 | Epilayer model. | 20 |
| 8 | Base resistance | 23 |
| 9 | Cut-off frequency | 26 |
| 10 | Temperature scaling rules. | 30 |
| 11 | Conversion of Mextram to Vbic95 parameters. | 35 |
| 12 | Conclusions | 39 |
| A | Appendix | 43 |

Distribution

1 Introduction

Recently a new bipolar transistor model Vbic95 (Vertical Bipolar Inter-Company model 1995) is introduced to become the new world wide standard for bipolar transistor modelling and characterization. The Vbic95 model is in many aspect compatible with the current aging standard, the Spice Gummel Poon (SGP) model. The model was officially released at the BCTM 1995 conference, and public domain model code and documentation are available on request from Colin McAndrew at mcandrew@sst.sps.mot.com. Commercial implementations of the model are being integrated into the circuit simulation/extraction tools of many CAD vendors.

The main improvements of the Vbic95 model over the SGP model are the explicit modelling of the parasitic PNP transistor, bias dependent Early voltages, modelling of the epilayer resistance (base push-out), avalanche multiplication and the extensive temperature mapping.

In this report the Vbic95 model release 1.1.4 is compared with the Philips bipolar transistor model Mextram. Also this model is public domain and model documentation [5] is available on request from Willy Kloosterman at mm9_mxt@natlab.research.philips.com

To compare both models easily the basic components of the Vbic95 model are implemented as a user defined model in the Philips proprietary circuit simulator Pstar including parameter conversion (see appendix A).

In the different sections the electrical equivalent circuit, the three junction capacitances, the output conductance, the collector, emitter, base and substrate current, the base and epilayer resistance model, the diffusion charges and the temperature scaling rules are compared.

2 Electrical equivalent network

The electrical equivalent network of the Mextram and Vbic95 model are shown in figures 1 and 2. The Vbic95 model has besides the electrical equivalent network also a thermal network and an excess phase network. In Mextram base charge partitioning is used to implement excess phase shift. The electrical equivalent network of both models consist of an intrinsic NPN transistor and a parasitic PNP transistor. In the Mextram model the PNP transistor may be split up in a sidewall and a floor component whereas in the Vbic95 model the PNP transistor has substrate and base series resistances. The representation of the elements is only for historical reasons somewhat different for both models. In the scheme below the corresponding element are summarized. In most cases the formulation of the elements are different.

$$\begin{aligned} I_{cc} &\equiv I_n \\ I_{be} &\equiv I_{b1} + I_{b2} \end{aligned}$$

$$\begin{aligned}
Q_{be} &\equiv Q_{te} + Q_{be} + Q_n \\
I_{gc} &\equiv I_{avl} \\
Q_{bc} &\equiv Q_{bc} + Q_{tc} + Q_{epi} \\
I_{be}^x &\equiv I_{b1}^S \\
Q_{be}^x &\equiv Q_{te}^S \\
R_{bi} &\equiv R_{bv} \\
R_{bx} &\equiv R_{bc} \\
R_{ci} &\equiv I_{c1c2} \\
R_{cx} &\equiv R_{cc} \\
I_{cc}^p &\equiv I_{sub} + XI_{sub} \\
I_{be}^p &\equiv I_{ex} + XI_{ex} + I_{b3} \\
I_{bc}^p &\equiv I_{sf} \\
Q_{be}^p &\equiv Q_{tex} + Q_{ex} + XQ_{tex} + XQ_{ex} \\
Q_{bc}^p &\equiv Q_{ts}
\end{aligned}$$

The elements I_{bc} , Q_{bc}^x , C_{beo} , C_{bco} , R_s and R_{bip} are not present in the Mextram model whereas the elements Q_{b1b2} (AC current crowding) and the diode between nodes $B1$ and $B2$ (DC current crowding) are not present in the Vbic95 model. In the Vbic95 model DC and AC current crowding have to be modelled with the sidewall components I_{be}^x and Q_{be}^x (see also the section base resistance).

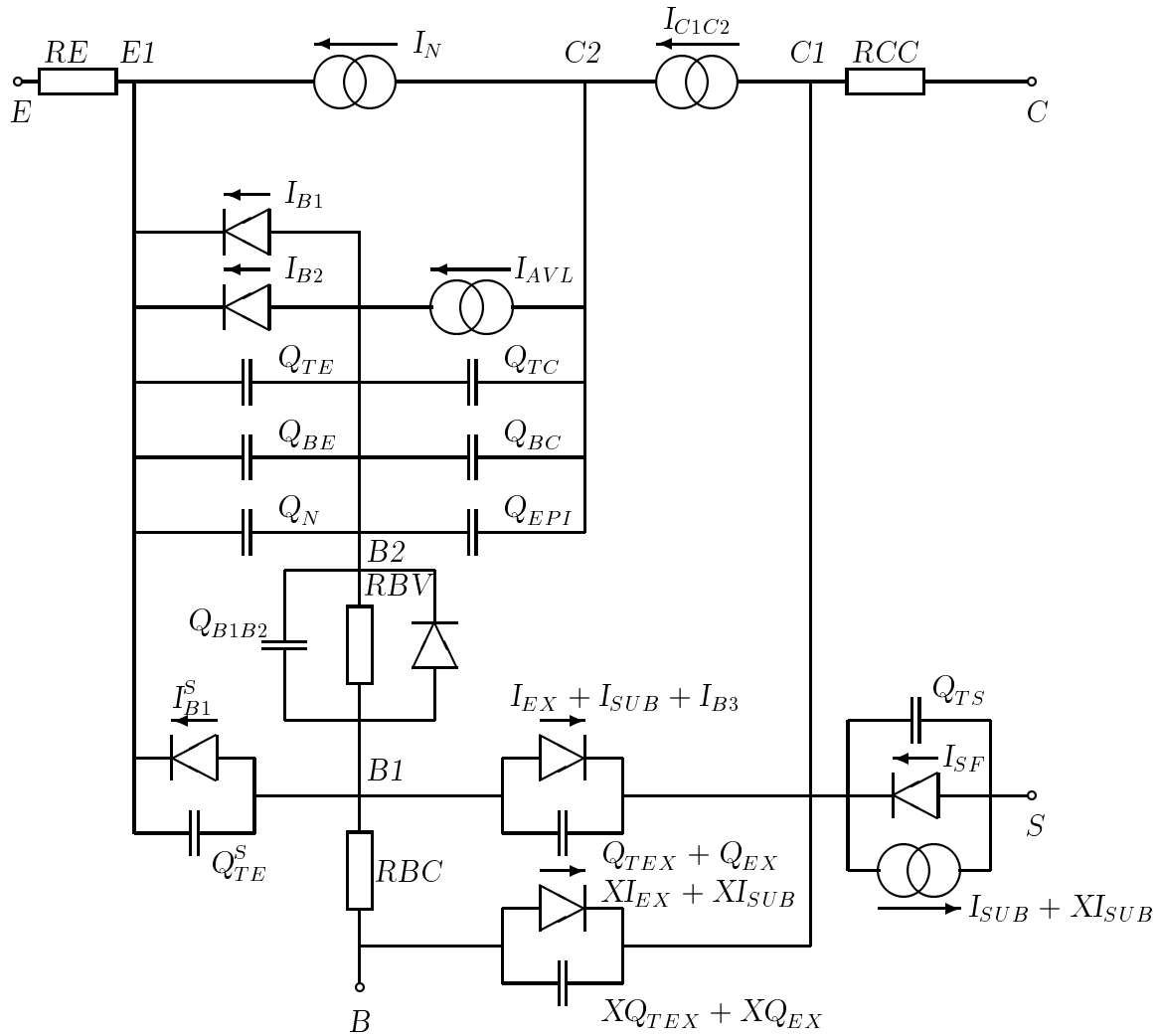
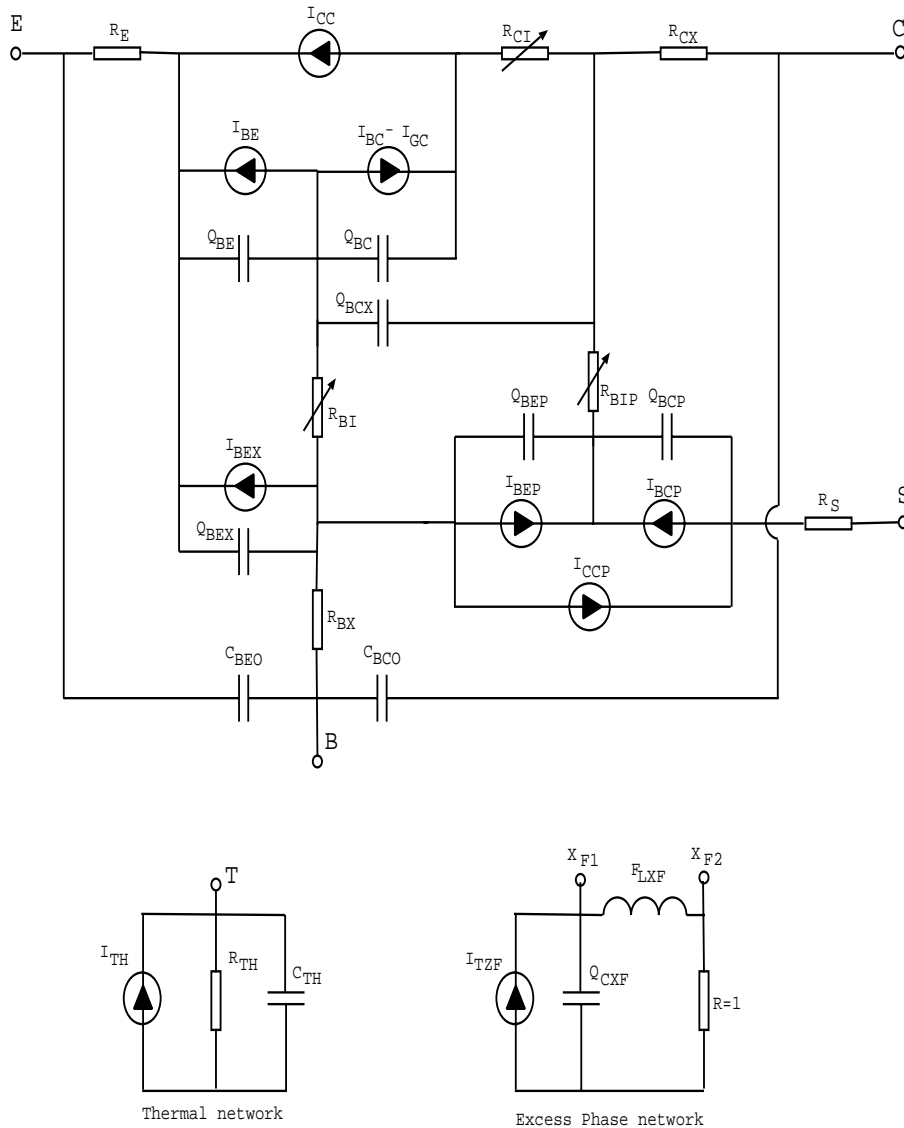


Figure 1: Equivalent network for Mextram

Figure 2: *Equivalent Network for Vbic95*

3 Depletion capacitances

Vbic95 describes the three junction capacitances (base-emitter, base-collector and collector-substrate) with the same equations whereas in Mextram the base-collector depletion capacitance differs from the other two capacitances. The parameter values of the b-e and s-c capacitance are identical in Vbic95 and Mextram however the parameter names are different; $PE = Vde$, $ME = Pe$, $Cjc^p = Cjs$, $PS = Vds$, $MS = Ps$. Be aware that the diffusion voltage in Vbic95 has the same name as the grading coefficient in Mextram. Vbic95 need two additional parameters (FC and AJ) to model the capacitance near the diffusion voltage (see figure 3). Parameter

FC defines the junction voltage ($FC \cdot PE$) where the capacitance is extrapolated or kept constant depending on the sign of parameter AJ . When AJ is negative the Spice Gummel Poon (SGP) approach is used to extrapolate the capacitance and if AJ is positive then the depletion charge is extrapolated (resulting in a constant capacitance). Now the value of AJ models the transition region. The transition region increases for larger values of AJ . Typical values used for AJ are in between 0.01 and 0.1. The parameter value of FC have to be around 0.9. The same parameter FC is used for the three junction capacitances whereas AJ may be specified for each junction (AJE , AJC , AJS). The b-e junction capacitance may be split in a floor and sidewall component as in the Mextram model. The sidewall component is $1 - WBE$. The Vbic95 parameter WBE therefore becomes $1 - XCje$. Note that the base current component I_{be}^x in Vbic95 also depends on WBE whereas in Mextram a separate factor $XIbi$ is used.

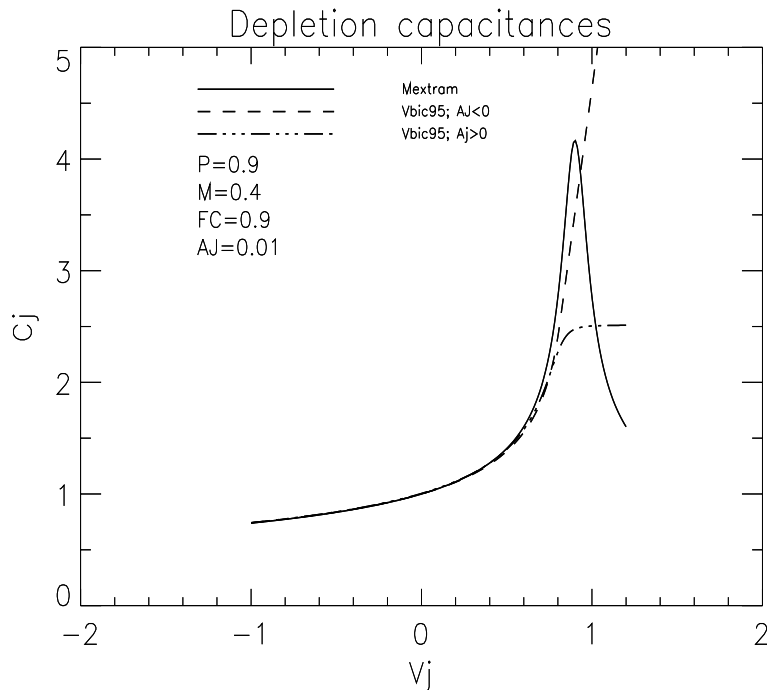


Figure 3: Comparison of the depletion capacitance model of Vbic95 and Mextram for the b-e and s-c junction.

The b-c junction capacitance model in Mextram differs from the b-e and s-c junction capacitance model. The Mextram model takes into account the finite thickness of the epilayer and the influence of the collector current. As a consequence also the parameters are different. When we make the capacitance model similar for small collector currents and small base-collector voltages then the Vbic95 parameters becomes;

$$CJC \equiv XCjc \cdot Cjc$$

$$CJEP \equiv (1 - XCjc) \cdot Cjc$$

$$PC \equiv Vdc$$

$$MC \equiv (1 - Xp) \cdot Pc$$

In figure 4 the b-c capacitance is plotted for different current densities in the epilayer. The parameters used are listed in the plot. In the Mextram model the b-c capacitance underneath the emitter decreases with collector current. The minimum capacitance is given by the thickness of the epilayer W_{epi} and equals to $A_{em} \cdot \epsilon / W_{epi} = X_p \cdot XCjc \cdot Cjc$. In the Vbic95 model the capacitance does not depend on the current density in the epilayer.

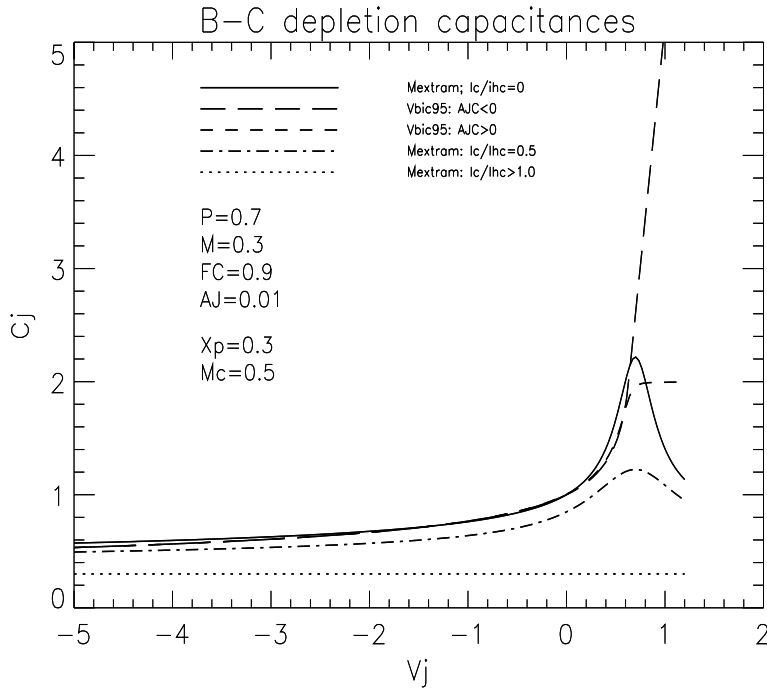


Figure 4: Comparison of the b-c depletion capacitance model of Vbic95 and Mextram for different current densities in the epilayer.

4 Early voltages

An important improvement of the Vbic95 model in comparison with the SGP model is the modelling of the Early effect (base width modulation). The SGP model has constant Early voltages. The forward and reverse Early voltage in Vbic95 and Mextram model are the same up to medium current levels. This makes it easy to convert the parameters;

$$VEF \equiv Qb0 / (XCjc \cdot Cjc)$$

$$VER \equiv Qb0 / ((1 - XCjc) \cdot Cjc)$$

The description of Early effect at higher collector current (high injection: $q_2 > 0$) is quite different. Now SGP and Mextram are more similar. The term q_b (see table 1) describes in the three models the combined effect of forward Early, reverse Early and high injection of the intrinsic NPN transistor.

| | SGP | Vbic95 | Mextram |
|-------|---|---|-----------------------------------|
| q_1 | $\frac{1}{1 - \frac{V_{be}^i}{V_{AR}} - \frac{V_{bc}^i}{V_{AF}}}$ | $1 + \frac{V_{te}}{VER} + \frac{V_{tc}}{VEF}$ | $1 + \frac{Q_{te} + Q_{tc}}{Qb0}$ |
| q_2 | $\frac{I_f}{IKF} + \frac{I_r}{IKR}$ | $\frac{I_f}{IKF} + \frac{I_r}{IKR}$ | $\frac{Q_{de} + Q_{dc}}{Qb0}$ |
| q_b | $q_1 \cdot \left(\frac{1 + \sqrt{1 + 4 \cdot q_2}}{2} \right)$ | $\frac{q_1 + \sqrt{q_1^2 + 4 \cdot q_2}}{2}$ | $q_1 \cdot (1 + q_2)$ |
| I_c | $\frac{I_f - I_r}{q_b}$ | $\frac{I_f - I_r}{q_b}$ | $\frac{I_f - I_r}{q_b}$ |

Table 1: Model equations used in the Spice Gummel-Poon (SGP), Vbic95 and Mextram model to describe the Early effect and high injection effect.

The terms I_f and I_r are the ideal forward and reverse current respectively. The collector current I_c becomes for all models $(I_f - I_r)/q_b$. In this report the forward Early voltage Ea_f and the reverse Early voltage Ea_r are defined as;

$$Ea_f = I_c / \frac{\partial I_c}{\partial V_{bc}^i}$$

$$Ea_r = I_c / \frac{\partial I_c}{\partial V_{be}^i}$$

In figure 5 the forward Early voltage is plotted as a function of the internal collector junction voltage V_{bc}^i with a constant value of $0.6V$ for the internal base-emitter voltage V_{be}^i . In this case the term $q_2 \approx 0$ (no high injection effects) and we see that Vbic95 and Mextram behaves similar and that the Early voltage of the SGP model only slightly increases with collector voltage. The difference at higher collector voltage between the Vbic95 and the Mextram model is due to the different collector depletion charge models. For actual devices the Early voltage will decrease strongly at high collector voltage due to avalanche multiplication in the collector. Therefore this difference will not be seen in the output conductance of actual devices.

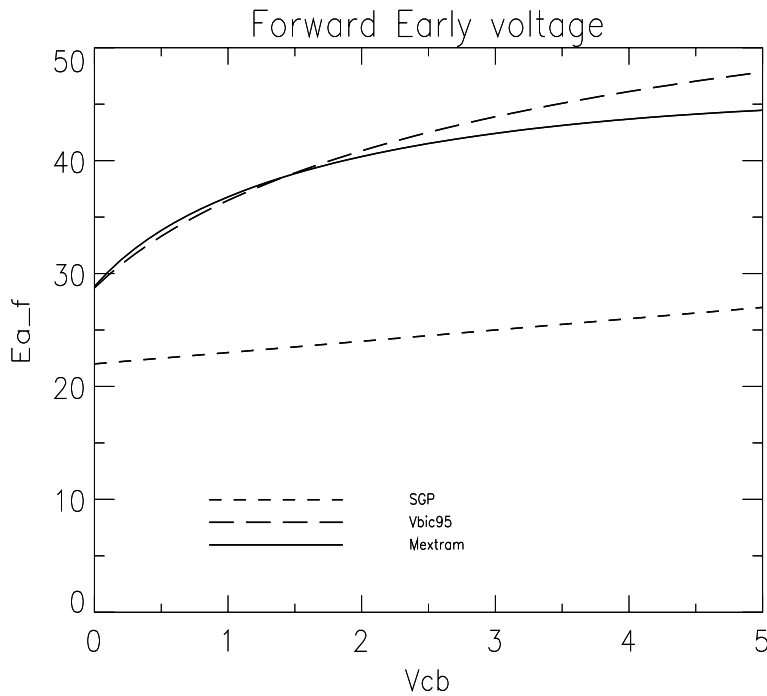


Figure 5: Comparison of the forward Early voltage of the SGP, Vbic95 and Mextram model at small collector currents. The Early parameters are taken the same for the three models ($VAF=VEF=25V$, $VAR=VER=5V$.)

In figure 6 the forward Early voltage is plotted versus the internal b-e junction voltage with $V_{cb}^i = 0V$. For the SGP model the Early voltage decreases with VAF/q_1 . For the Mextram model and Vbic95 model the Early voltage initially increases with $VEF \cdot q_1$. In the Vbic95 model the Early voltage goes to infinity when the collector current passes the knee current IKF . The reason is that above IKF the q_2 term dominates the q_b term and q_2 does not depend on the collector voltage (assume $I_r = 0$). In the Mextram model the Early voltage increases at higher V_{be}^i due to current modulation in the collector space charge region. When the collector current approach and exceed I_{hc} (critical current for hot carrier behavior: $I_{hc} = A_{em} \cdot q \cdot N_{epi} \cdot v_{sat}$) the collector space charge region extend into the buried layer and the collector capacitance becomes ϵ/W_{epi} . Therefore the Early voltage increases to $q_1 \cdot VEF/XP$ when the collector current passes I_{hc} . For actual devices the Early voltage will decrease at high V_{be}^i due to base-push out ($I_r \neq 0$). Base-push out is taken into account both in the Vbic95 and Mextram model. Summarizing, up to medium current levels (no high injection and base push out) the Early voltages in Mextram and Vbic95 are similar. In the Vbic95 model the Early voltage becomes infinity above the knee current and in the Mextram model the Early voltage increases with a factor $1/XP$ when the collector current passes I_{hc} .

The reverse Early voltage behaves like the forward Early voltage at small current levels. (see figure 7). The reverse Early voltage slightly increases with the reverse biased junction voltage. At high current levels both models behaves differently. In

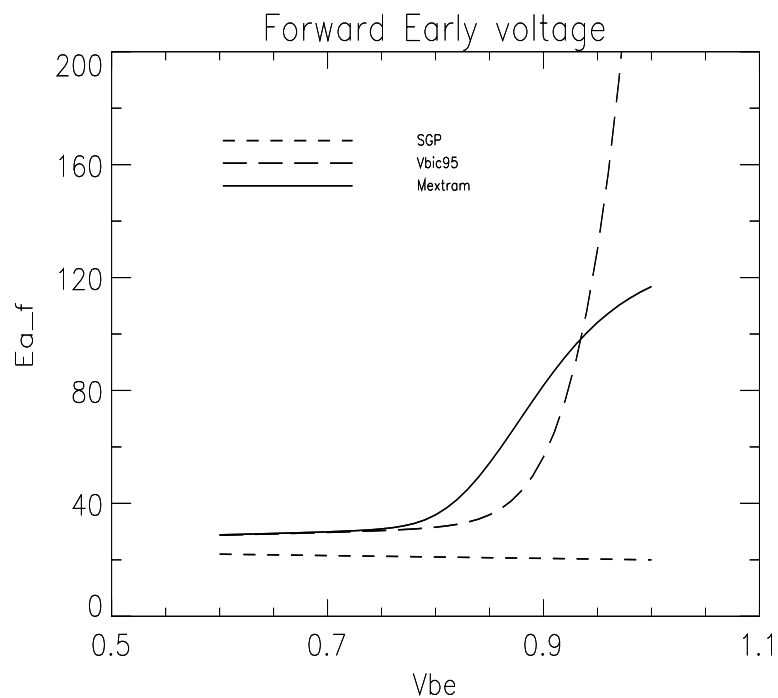


Figure 6: Comparison of the forward Early voltage of the SGP, Vbic95 and Mextram model with increasing collector current. In the SGP model the Early voltage decreases proportional with q_1 . For the Vbic95 model the increase at higher V_{be} is caused by high injection in the base and in the Mextram model by modulation of the collector capacitance underneath the emitter.

the Mextram model the reverse Early voltage doesn't increase significantly with forward biased junction voltage (reverse mode of operation) because the base-emitter depletion charge Q_{te} doesn't depend on I_e , while in the Vbic95 model the reverse Early voltage increases due to high injection as in the forward mode of operation.

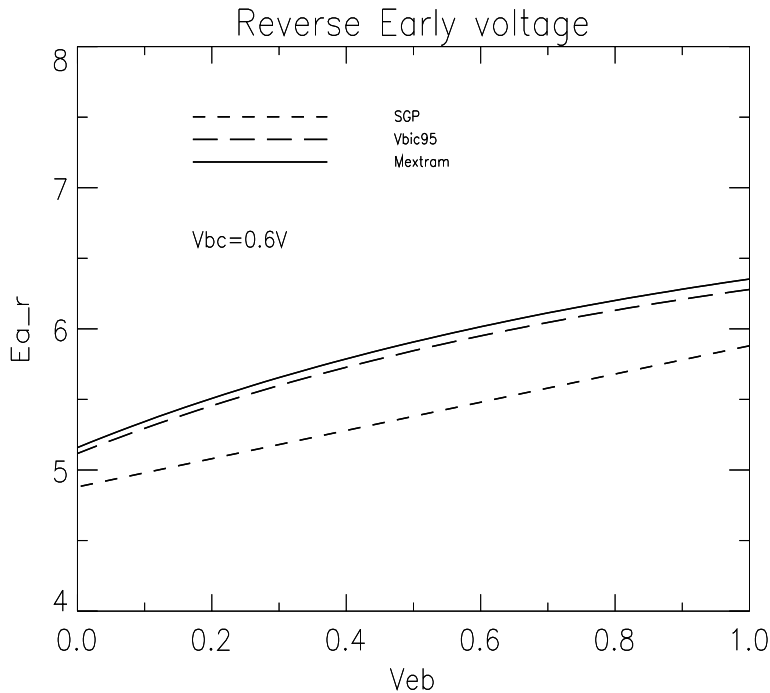


Figure 7: Comparison of the reverse Early voltage of the SGP, Vbic95 and Mextram model with increasing emitter voltage.

5 Forward current gain

In this section the forward current gain of the Vbic95 and Mextram model excluding base-push out are compared. Base-push out is caused by the collector series resistances and the influence on the transistor characteristics will be shown in the section about the epilayer modelling. First the description of the collector current and base current components will be explained in more detail and then the influence on the current gain.

5.1 Collector current

The modelling of the collector current is given in table 1. In the Vbic95 and Mextram model the description of the forward and reverse Early effect are similar and therefore also the collector current will be more or less the same when we exclude high injection ($q_2 = 0$). For advanced devices the reverse Early effect (V_{te}/VER , Q_{te}/Q_{b0}) decreases the ideal collector current I_f significantly up to 25%. In the

Vbic95 model the non-ideal exponential behavior of the collector current may be described also by the forward emission coefficient NF . In most cases NF will be close to unity when the device temperature, the b-e and b-c capacitance parameters are well defined. The modelling of high injection is quite different for the Vbic95 and Mextram model. The Vbic95 model posses two knee currents (IKF , IKR) whereas the Mextram model uses one knee current (IK) and the built-in electric field (ETA) of the base doping profile. In figure 8 the relative difference between the collector current in the Vbic95 and Mextram model is plotted versus V_{be}^i for different values of the built-in factor ETA of the Mextram model. The parameter value for IKF and IK are the same. The Early effect is excluded ($q_1 = 1$). In the transition region ($I_c \approx IK$) the differences may be up to 10% in the collector current.

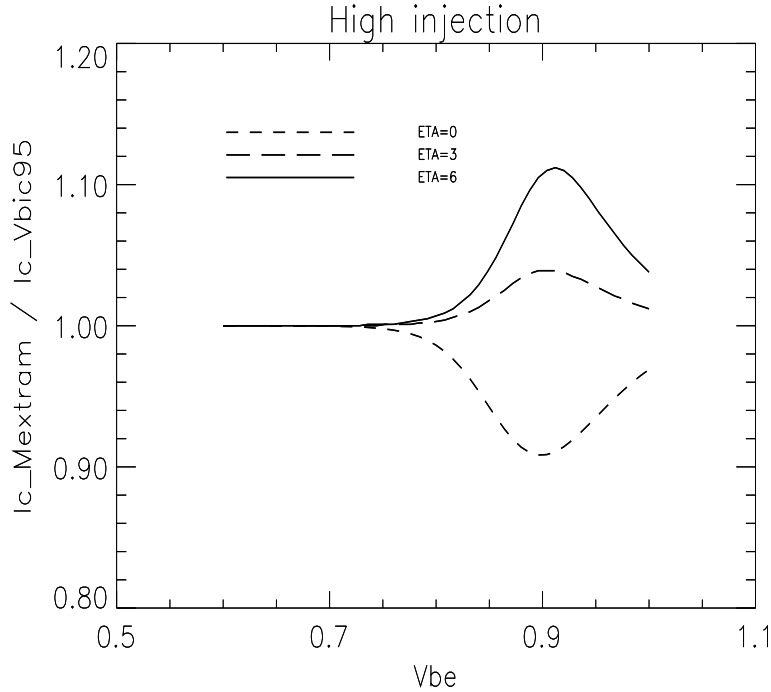


Figure 8: Comparison of the normalized collector current in the high injection regime for the Vbic95 and Mextram model. For the Mextram model different values for the built-in field ETA of the active base are used. The Early effect is excluded ($q_1 = 1$)

The differences becomes much larger if we take into account the Early effect. At higher current densities the q_b term in the Vbic95 model becomes equal to the q_2 term whereas in the SGP and Mextram model q_b becomes approximately $q_1 \cdot q_2$. Therefore the collector current in the Vbic95 model may be up to 40 % larger in comparison with the SGP and Mextram model at high current densities depending mainly on the reverse Early voltage. (see figure 9). The resulting increase in forward gain can be reduced by splitting the base current in a sidewall and floor component to enlarge the base current.

The Mextram model uses the base diffusion charges Q_{de} and Q_{dc} to account for high injection effects (see table 1). The same charges Q_{de} and Q_{dc} also determine the

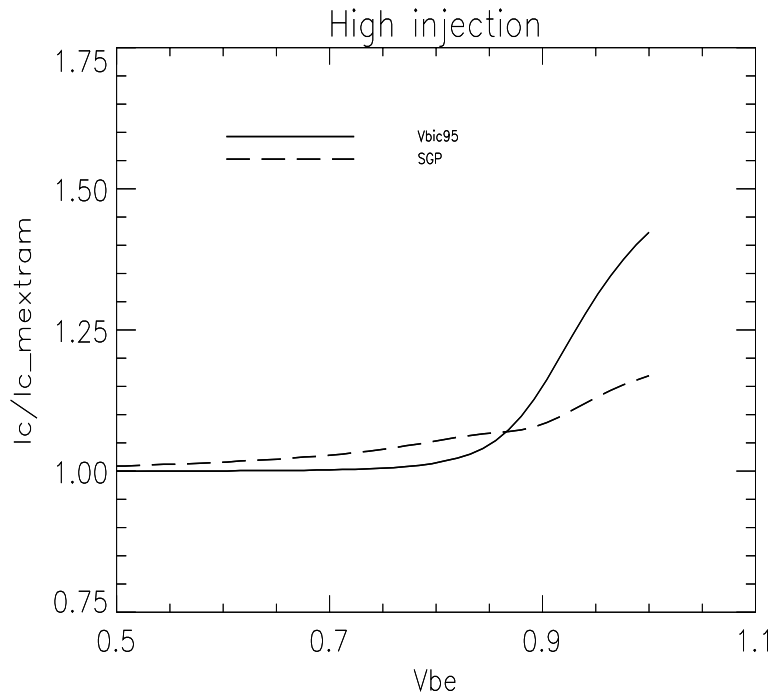


Figure 9: Comparison of normalized Vbic95 and SGP collector current with Mextram including the Early effect and high injection and without base-push out. The Vbic95 collector current may be up to 40% higher.

base transit time. This has its impact on the determination of parameters and will be explained in more detail in the section about the cut-off frequency. In Mextram and Vbic95 the collector epilayer resistance has a large influence on the gain roll-off both in the forward and reverse mode of operation. This will be explained later in more detail.

5.2 Forward base current

The forward base current is built up by a non-ideal, a floor and a sidewall component. (see table 2). The Vbic95 non-ideal base current is equal to the SGP non-ideal base current using the same parameters. The Mextram non-ideal base current description is quite different but the calculated roll-off of the gain is similar to the Vbic95 model (see figure 10). When parameter VLF is sufficient small ($VLF \leq 0.4V$) then $I_{be}^n \approx I_{bf}$ and $NEN \approx 2$. To convert Mextram parameters to Vbic95 parameters the best solution is to calculate two data point (e.g. 0.5V, 0.7V) and calculate then I_{be}^n and NEN . The description of the ideal component I_{be}^i is identical but the parameters are different. In the Vbic95 model the base saturation current I_{be}^i is taken as parameter whereas in the Mextram model the intrinsic gain B_f is the parameter ($B_f = I_s/I_{be}^i$). In addition for the Vbic95 model a b-e emission coefficient (NEI) may be specified.

| | Vicb95 | Mextram |
|------------|--|--|
| I_{be}^n | $I_{be}^n \cdot \left(\exp \left(\frac{V_{be}^i}{NEN \cdot V_t} \right) - 1 \right)$ | $Ib_f \cdot \left\{ \frac{\exp \left(\frac{V_{be}^i}{V_t} \right) - 1}{\exp \left(\frac{V_{be}^i}{2 \cdot V_t} \right) + \exp \left(\frac{V_{LF}}{2 \cdot V_t} \right)} \right\}$ |
| I_{be}^i | $WBE \cdot I_{be}^i \cdot \left(\exp \left(\frac{V_{be}^i}{NEI \cdot V_t} \right) - 1 \right)$ | $\frac{(1 - XIBI) \cdot I_s}{Bf} \cdot \left(\exp \left(\frac{V_{be}^i}{V_t} \right) - 1 \right)$ |
| I_{be}^x | $(1 - WBE) \cdot I_{be}^i \cdot \left(\exp \left(\frac{V_{be}^x}{NEI \cdot V_t} \right) - 1 \right)$ | $\frac{XIBI \cdot I_s}{Bf} \cdot \left(\exp \left(\frac{V_{be}^x}{V_t} \right) - 1 \right)$ |

Table 2: Model equations used in the Vbic95 and Mextram model to describe the forward base current.

The difference in base current components in the SGP, Vbic95 and Mextram model are small. The difference in current gain is larger due to the different modelling of the collector current. Up to medium current levels the SGP current gain is somewhat higher due to a smaller q_1 . At high current levels and taking into account only high injection (no base push-out) the gain in the Vbic95 model is larger due to the larger collector current (using same parameters). This means that the extracted knee current IKF in the Vbic95 model becomes somewhat smaller in comparison with the SGP and Mextram model. For actual advanced bipolar transistors used for analogue application the gain roll-off at high current densities is mainly caused by base push-out. In many cases only the initial roll-off of the gain is due to high injection effects.

In the Vbic95 (fraction $1 - WBE$) and Mextram model (fraction $XIBI$) the base current may be split-up in a base-emitter sidewall component and a base-emitter floor component. The sidewall component depends on the voltage at the base-emitter sidewall (V_{be}^x). In the Vbic95 model the distribution of the base-emitter depletion charge and base current in a sidewall and floor component also serves as a first order AC and DC current crowding model. In the Mextram model there are additional base resistance components to describe DC and AC current crowding. Because there are no collector b-e sidewall components in Vbic95 and Mextram model the influence on the roll-off of the forward gain may be quite large (up to 25%) depending on the base resistance. It may have a large impact on the high current model parameters (knee current, epilayer parameters) during parameter extraction.

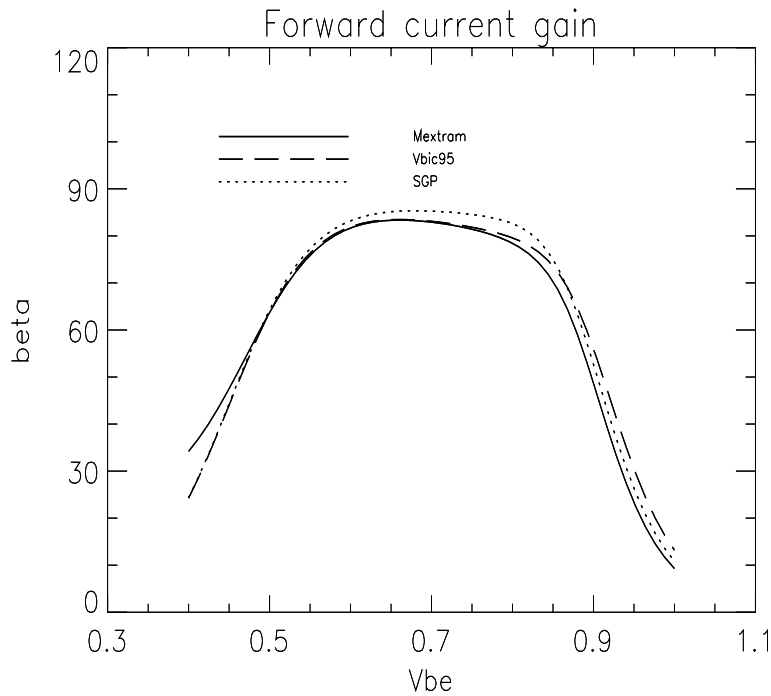


Figure 10: Comparison of the SGP, Vbic95 and Mextram forward current gain excluding base push-out. The difference in gain is mainly due to the difference in collector current. All series resistances are zero.

6 Reverse current gain

The base current in de reverse mode of operation ($V_{bc} > 0$, $V_{be} \leq 0$) is made up mainly by the collector current of the parasitic PNP transistor and in less extent to the reverse base current of the NPN transistor. The PNP transistor is not present in the SGP model and therefore the behavior of the reverse gain may be quite different. In general at low current densities the differences are small and comparable to the differences seen in the forward mode of operation. At medium and high reverse currents the difference may be larger between the three models. This will have also its impact on the on-resistance ($V_{ce_{sat}}$) at small values of V_{ce} . In the next sections the emitter, the substrate and intrinsic base currents will be explained in more detail.

6.1 Emitter current of the reverse Gummel plot.

The description of the emitter current in the reverse mode of operation is also given by table 1. The different formulation of the Early effect (q_1) and high injection effect (q_2) results in the same kind of deviations between the three models as in the forward mode of operation. The present of the collector epilayer in the Vbic95 and Mextram model may decreases the emitter current considerably and therefore the reverse current gain. In the reverse mode of operation the description of the

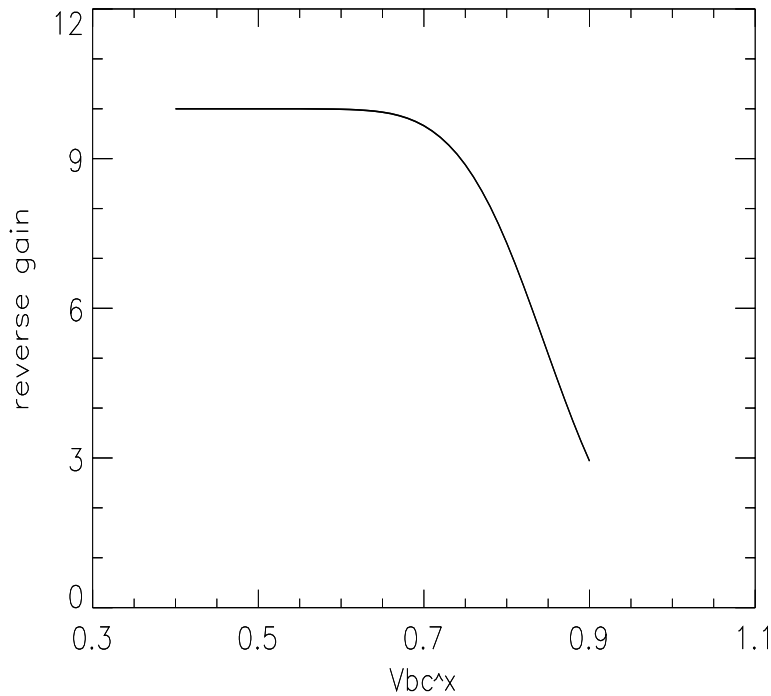


Figure 11: *The decrease of the reverse current gain due to the resistivity of the collector epilayer.*

current through the epilayer is the same for the Mextram and Vbic95 model when we exclude velocity saturation (VO_{high}) in the Vbic95 model. (see equation 1).

$$\begin{aligned}
 I_{epi}^0 &= \frac{E_c + V_{bc}^i - V_{bc}^x}{RCI} & (1) \\
 E_c &= V_t \cdot \left(K_i - K_x - \ln \frac{1 + K_i}{1 + K_x} \right) \\
 K_i &= \sqrt{1 + GAMM \cdot \exp(V_{bc}^i/V_t)} \\
 K_x &= \sqrt{1 + GAMM \cdot \exp(V_{bc}^x/V_t)} \\
 GAMM &= 4 \cdot \exp(-V_{dc}/V_t)
 \end{aligned}$$

In the Mextram model the collector diffusion voltage V_{dc} is the model parameter and in Vbic95 $GAMM$. Therefore the collector diffusion voltage in the Mextram model is a very important parameter and in most cases this parameter is obtained from the transistor operating in quasi-saturation (base push-out regime). In the Vbic95 model the collector diffusion voltage is only used in the capacitance and Early effect model and an additional parameter $GAMM$ in the collector epilayer model. To illustrate the effect of the resistivity of the epilayer on the reverse current gain the emitter and base current are calculated according to:

$$\begin{aligned}
 I_e &= I_s \cdot \left\{ \exp\left(\frac{V_{bc}^i}{V_t}\right) - 1 \right\} \\
 I_b &= \frac{I_s}{B_r} \cdot \left\{ \exp\left(\frac{V_{bc}^x}{V_t}\right) - 1 \right\} \\
 I_e &= I_{epi}^0
 \end{aligned}$$

and using the following parameters: $RCI = 100\Omega$, $Vdc = 0.7V$ and $B_r = 10$. The calculated gain is shown in figure 11. Without the collector epilayer resistance the reverse gain will be constant. Due to the presence of the epilayer the knee current in the Vbic95 model will be larger than in the SGP model. The consequence is that the parameter IKR of the SGP model can not be used in the Vbic95 model. A better approximation is to make IKR equal to the forward knee current IKF in Vbic95. The emitter current in the Mextram model is somewhat smaller in comparison with the Vbic95 model due to the built-in electric field of the base (parameter ETA).

6.2 Substrate current.

The Vbic95 and Mextram model describes both the substrate current being the main current I_{cc}^p of the parasitic PNP transistor (see table 3). This parasitic PNP transistor is not present in the SGP model. In most cases the reverse current gain is reduced considerably by the substrate current.

For both models the substrate equations are similar but they are applied to different node voltages. In the Vbic95 model the substrate current may depend on the base-collector junction voltage underneath the emitter V_{bc}^i and the base-collector junction voltage besides the emitter V_{bc}^p . The distribution factor WSP is a parameter. The part originating from the intrinsic device may be obtained from the substrate current when the transistor is in quasi-saturation. In general for transistors with a buried collector layer the substrate current in the quasi-saturation mode is neglectable ($WSP \approx 1$). Also an emission coefficient NFP may be specified. The description of high-injection is the same for both components. For devices where the buried layer and collector plug does not surround completely the base area the substrate current may be very large. Then the base of the parasitic PNP device has a small Gummel number and the saturation current (I_s^p) is large. Also at relative small current densities the substrate current exhibit high injection. This is seen in the increase of the reverse gain at moderate base-collector voltages. In the Vbic95 model the knee current parameter is IKP and in the Mextram model IKS . In the Mextram model the knee of substrate current is projected on the emitter current and therefore $IKS = IKP \cdot I_s / I_s^p$. In the Vbic95 model at least the constant part of the base resistance RBX and the constant of the collector resistance RCX are in series with the p-n junction. This means that there will be a large voltage drop over the base and collector resistance at high reverse bias. Therefore in most cases the absolute value of the base and substrate current will be too small in the Vbic95 model in comparison with measured data. Also the on-resistance in the output

| | Vicb95 | Mextram |
|---------------|--|---|
| I_{tf}^p | $I_s^p \cdot \left\{ WSP \cdot \exp\left(\frac{V_{be}^p}{NFP \cdot V_t}\right) + (1 - WSP) \cdot \exp\left(\frac{V_{bc}^i}{NFP \cdot V_t}\right) - 1 \right\}$ | $I_{ss} \cdot \left\{ \exp\left(\frac{V_{be}^p}{V_t}\right) - 1 \right\}$ |
| I_{tf}^{px} | — | $I_{ss} \cdot \left\{ \exp\left(\frac{V_{bc}^{px}}{V_t}\right) - 1 \right\}$ |
| I_{bc}^p | $I_s^p \cdot \left\{ \exp\left(\frac{V_{bc}^p}{NFP \cdot V_t}\right) - 1 \right\}$ | $I_{ss} \cdot \left\{ \exp\left(\frac{V_{bc}^p}{V_t}\right) - 1 \right\}$ |
| q_b^p | $\frac{1 + \sqrt{1 + 4 \cdot \frac{I_{tf}^p}{IKP}}}{2}$ | $\frac{1 + \sqrt{1 + 4 \cdot \frac{I_s \cdot I_{tf}^p}{I_{ss} \cdot IK S}}}{2}$ |
| q_b^{px} | — | $\frac{1 + \sqrt{1 + 4 \cdot \frac{I_s \cdot I_{tf}^{px}}{I_{ss} \cdot IK S}}}{2}$ |
| I_{cc}^p | $\frac{I_{tf}^p - I_{bc}^p}{q_b^p}$ | $\frac{(1 - XEXT) \cdot I_{tf}^p}{q_b^p} + \frac{XEXT \cdot I_{tf}^{px}}{q_b^{px}}$ |

Table 3: Model equations used in the Vbic95 and Mextram model to describe the substrate current I_{cc}^p .

characteristic I_c versus V_{ce} is affected. In the Mextram model the parasitic PNP may be distributed over the constant base resistance. In the device cross section it can be seen as a PNP formed by the bottom area of the base and a second one formed by the sidewall area of the base region. The bottom part depends on voltage V_{be}^p being the junction voltage $V_{b_1c_1}$ and the outer part on voltage V_{be}^{px} being the voltage V_{bc_1} (see equivalent network figure 1). The partitioning factor $XEXT$ is obtained from the high current regime of the reverse Gummel plot. Notice that the base-collector capacitance follows the same partitioning. The partitioning of the base-collector capacitance is important in the forward mode of operation at high frequencies. The Vbic95 and Mextram model of the substrate current becomes the same when $WSP = 1$, $NFP = 1$ and $XEXT = 0$. The parameters can easily be converted because they are extracted at small up to medium current levels.

6.3 Reverse base current.

In the Vbic95 model the reverse base current may consist of two components being the current of the b-c junction underneath the emitter (I_{bc}^i) and the current of the b-c junction besides the emitter (I_{be}^{ip}) respectively (see table 4). Each component may have an ideal and non-ideal part. In Mextram the reverse base current is distributed over the constant part of the base resistance and takes into account high injection effects and the non-ideal reverse base current depends only on the V_{be}^p voltage.

The current (I_{bc}^p) of the forward biased substrate-collector junction can be described accurately in the Vbic95 model. In Mextram this current can not be really modelled but only a signal current is added to give a serious warning for the normally undesired forward biasing of the substrate-collector junction. The partitioning of the base current in Vbic95 over I_{bc}^i and I_{be}^{ip} may be obtained from scaling of devices with different emitter and collector areas. When a substantial part of the base current is assigned to I_{bc}^i (parameters IBCI and IBCN) the output conductance may decrease considerably in quasi-saturation (I_c versus V_{ce}) when the transistor is biased with constant base current. In quasi-saturation the internal base-collector junction becomes forward biased and if IBCI and IBCN are comparable with IBEL and IBEN then a substantial part of the base current will flow into the collector and the internal base-emitter junction voltage decreases resulting in a decrease of the collector current. Also self heating may have a large effect on the output conductance especially when the base of the transistor is biased with a voltage source. In Vbic95 the constant part of the base and collector resistances are in series with the internal b-c junction and this will result in a large voltage drop over these resistances at high reverse bias. Therefore in many cases the calculated reverse currents in Vbic95 (emitter, base and substrate) will be too small. Nevertheless the reverse gain will be sufficient good because all currents are affected in the same way. The increase of the reverse gain at small current levels is due to the non-ideal reverse base current. The increase at medium current levels is in many cases due to high injection of the substrate current. The decrease of the reverse gain at high reverse bias is mainly caused by the resistivity of the epilayer and in less extent by high injection. Therefore first the parameters of the epilayer model and substrate current have to

| | Vicb95 | Mextram |
|---------------|---|---|
| I_{bc}^i | $IBCI \cdot \left\{ \exp \left(\frac{V_{bc}^i}{NCI \cdot V_t} \right) - 1 \right\} +$ $IBCN \cdot \left\{ \exp \left(\frac{V_{bc}^i}{NCN \cdot V_t} \right) - 1 \right\}$ | — |
| I_{be}^{ip} | $IBEIP \cdot \left\{ \exp \left(\frac{V_{be}^p}{NCI \cdot V_t} \right) - 1 \right\} +$ $IBENP \cdot \left\{ \exp \left(\frac{V_{be}^p}{NCN \cdot V_t} \right) - 1 \right\}$ | $\frac{(1 - XEXT)}{BRI} \cdot \left\{ \frac{alb + nb_{ex}}{ahb + nb_{ex}} \cdot \frac{I_K}{ahb} \cdot nb_{ex} - I_s \right\}$ $+ Ib_r \cdot \left\{ \frac{\exp \left(\frac{V_{bc}^p}{V_t} \right) - 1}{\exp \left(\frac{V_{bc}^p}{2 \cdot V_t} \right) + \exp \left(\frac{V_{LR}}{2 \cdot V_t} \right)} \right\}$ $nb_{ex} = 2 \cdot alb \cdot g_1 / \left(1 + \sqrt{1 + 4 \cdot g_1} \right)$ $g_1 = (I_s / I_K) \cdot (aho / alb)^2 \cdot \exp(V_{be}^p / V_t)$ |
| I_{be}^{xp} | — | $\frac{XEXT}{BRI} \cdot \left\{ \frac{alb + xnb_{ex}}{ahb + xnb_{ex}} \cdot \frac{I_K}{ahb} \cdot xnb_{ex} - I_s \right\}$ $xnb_{ex} = 2 \cdot alb \cdot xg_1 / \left(1 + \sqrt{1 + 4 \cdot xg_1} \right)$ $xg_1 = (I_s / I_K) \cdot (aho / alb)^2 \cdot \exp(V_{be}^{xp} / V_t)$ |
| I_{bc}^p | $IBCIP \cdot \left\{ \exp \left(\frac{V_{bc}^p}{NCIP \cdot V_t} \right) - 1 \right\} +$ $IBCNP \cdot \left\{ \exp \left(\frac{V_{bc}^p}{NCNP \cdot V_t} \right) - 1 \right\}$ | $I_{ss} \cdot \left\{ \exp \left(\frac{V_{bc}^p}{V_t} \right) - 1 \right\}$ |

Table 4: Model equations used in the Vbic95 and Mextram model to describe the reverse base currents.

| | Vicb95 | Mextram |
|-----------|---|---|
| I_{epi} | $\frac{I_{epi}^0}{\sqrt{1 + \left(\frac{I_{epi}^0}{I_{epi}^s}\right)^2}}$ | $I_{low} + S_f \cdot \frac{V_{epi} - I_{low} \cdot Rcv \cdot \left(1 - \frac{X_i}{W_{epi}}\right)}{SCRcv \cdot \left(1 - \frac{X_i}{W_{epi}}\right)^2}$ |
| | $I_{epi}^s = \frac{V0}{RCI} + \frac{\sqrt{V_{epi}^2 + 0.01}}{2 \cdot RCI \cdot HRCF}$ | $I_{low} = \frac{Ihc \cdot V_{epi}}{V_{epi} + Ihc \cdot Rcv \cdot \left(1 - \frac{X_i}{W_{epi}}\right)}$ |
| | $I_{epi}^0 = \frac{E_c + V_{epi}}{RCI}$ | $\frac{X_i}{W_{epi}} = \frac{E_c}{I_{epi} \cdot Rcv}$ |
| | | $S_f = 1 + \frac{2 \cdot Sfh}{1 + Sfh} \cdot \frac{X_i}{W_{epi}}$ |
| | | Substitution of I_{low} and X_i/W_{epi} leads to a cubic equation for I_{epi} . |

Table 5: Description of velocity saturation in the Vbic95 and Mextram model. E_c is defined by equation 1.

be extracted before we can describe the reverse current gain. To convert Mextram parameters to Vbic95 parameters we have to set IBCI and IBCN to zero and IBEIP to I_s/BRI . The non-ideal reverse base current component of I_{be}^p can be converted in the same way as the forward non-ideal component.

7 Epilayer model.

The description of the resistance of the epilayer in Vbic95 and Mextram are both based on the Kull [2] formulation. A detailed derivation of the Mextram epilayer model including velocity saturation and current spreading is published in [3]. Therefore in this report only the results of the models are compared. When we exclude velocity saturation in Kull, Vbic95 and Mextram then the bias dependent epilayer resistance of all the three models are the same and equal to I_{epi}^0 as defined by equation 1. The differences arise when we include velocity saturation.

The parameters of both models can simply be converted when we take the same transition voltage for velocity saturation and space charge resistance;

$$\begin{aligned} RCI &\equiv Rcv \\ V0 &\equiv Ihc \cdot Rcv \end{aligned}$$

$$HRCF \equiv \frac{SCR_{cv}}{2 \cdot R_{cv}}$$

$$GAMM \equiv 4 \cdot \exp(-V_{dc}/V_t)$$

In figure 12 the internal base-collector junction voltage is plotted as a function of the collector current. When we use the same parameters then the resistance of the epilayer is somewhat higher in Mextram and therefore the onset for quasi-saturation is reached at a smaller collector current. In quasi-saturation the internal junction voltage decreases slightly with current.

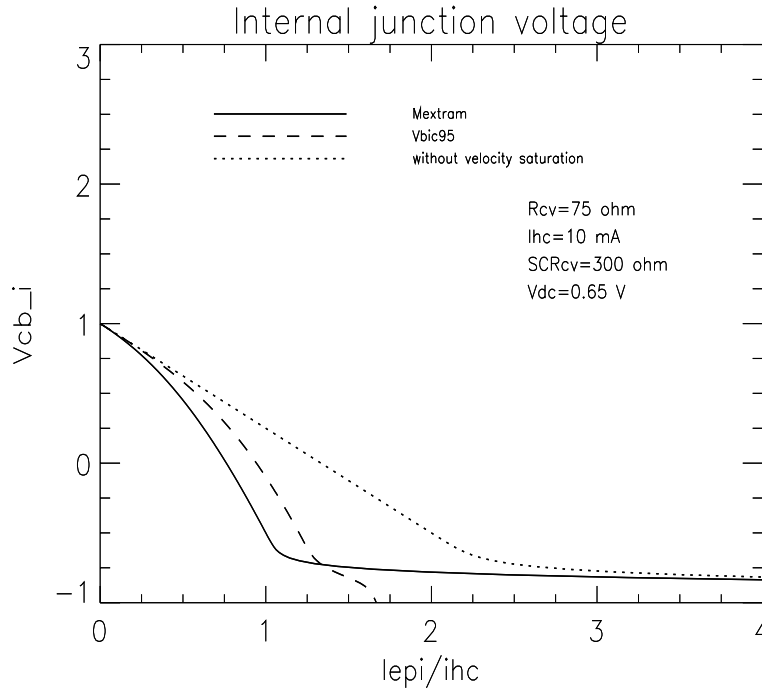


Figure 12: Comparison of the internal junction voltage V_{bc}^i for Vbic95 and Mextram using the same epilayer parameters.

To illustrate the impact of velocity saturation on quasi-saturation also the results are shown when we exclude velocity saturation. Now at much higher collector current ($I_c \approx (V_{cb_w} + V_{dc})/R_{cv}$) the internal junction voltage becomes forward biased due to the ohmic voltage drop. The effect of velocity saturation in the collector epilayer therefore is that it increases the quasi-saturation regime to lower collector currents and higher collector voltages. For Vbic95 the onset of quasi-saturation is reached at a somewhat higher current. However with increasing collector current the internal junction voltage doesn't approach the case without velocity saturation as it should be. This behavior is observed clearly when we plot the collector resistance (see figures 13 and 14) for the three cases. The differential resistances initially increases with collector current due to velocity saturation and decreases when the transistor enters quasi-saturation. However in strong quasi-saturation the differential resistance starts to increase for the Vbic95 model. This can not be true device

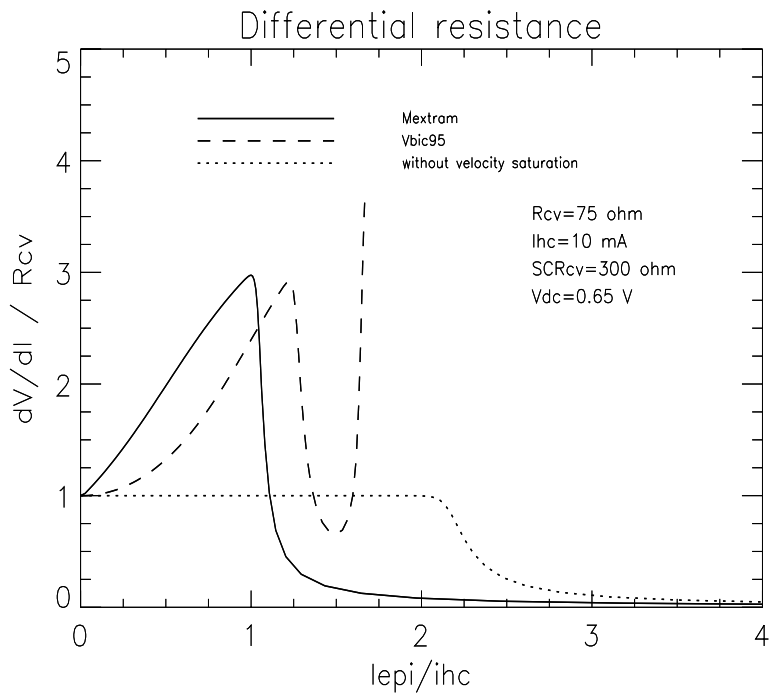


Figure 13: Comparison of the differential resistance for the Vbic95 and Mextram model.

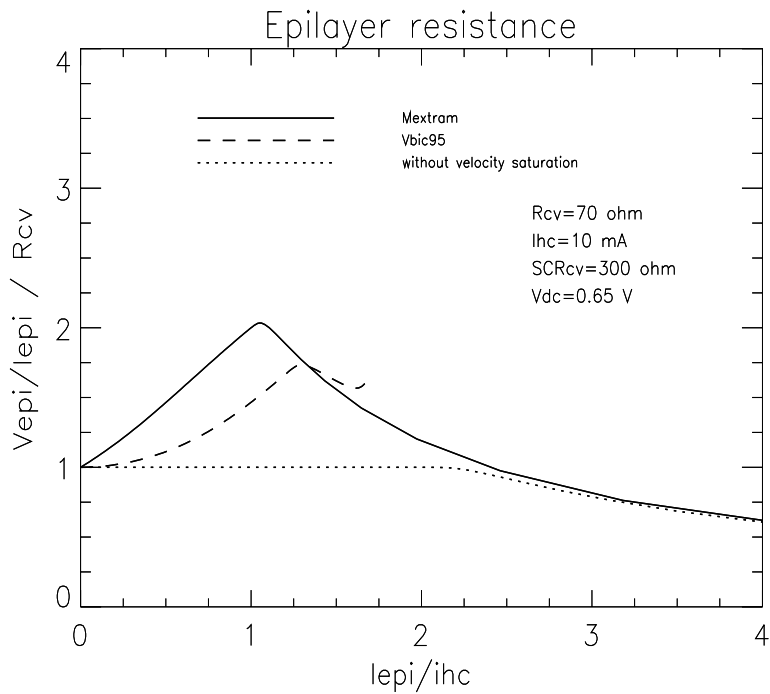


Figure 14: Comparison of the DC epilayer resistance of the Vbic95 and Mextram model

| | Vicb95 | Mextram |
|---------------|-------------------------------------|--|
| $I_{b_1 b_2}$ | $V_{b_1 b_2} \cdot \frac{q_b}{RBI}$ | $\frac{q_b}{3 \cdot RBV} \cdot \left(2 \cdot V_t \left(\exp \left(\frac{V_{b_1 b_2}}{V_t} \right) - 1 \right) + V_{b_1 b_2} \right)$ |
| $Q_{b_1 b_2}$ | – | $\frac{V_{b_1 b_2}}{5} \cdot \left(\frac{\partial Q_{TE}}{\partial V_{b_2 e_1}} + \frac{\partial Q_{BE}}{\partial V_{b_2 e_1}} + \frac{\partial Q_N}{\partial V_{b_2 e_1}} \right)$ |

Table 6: Description of the base resistance in the Vbic95 and Mextram model.

behavior. An accurate modelling of the onset for quasi-saturation (or base widening) is important because the degradation of current gain and cut-off frequency at low collector voltages is initiated by the collector resistance. To which extend the shown inordinate increase of the differential resistance in strong quasi-saturation hampers the suitability of the Vbic95 epilayer model is difficult to answer. The limitations becomes more prominent for thick ($> 1\mu m$) and low doped ($< 5 \cdot 10^{16}$) epilayers. I think a work around is to postpone velocity saturation in the Vbic95 model (set V_0 sufficient high) and use the ohmic collector resistance RCI and the knee current IKF to describe the current gain roll off.

A more general problem is the monotony of the output conductance (Early voltage) when an epilayer is present in a compact model. In Vbic95 and Mextram the Early voltage depends on the internal base-collector junction voltage and the shape of capacitance curve. When the transistor enters quasi-saturation the internal junction voltage becomes forward biased and the capacitance increases while the Early voltage decreases. In quasi-saturation the internal junction voltage becomes more or less constant and now the base-collector current (I_r) decreases the collector current and therefore the output conductance. For low doped epilayers parameter $GAMM$ is small and this may result in an initial increase of the output conductance in the transition region to quasi-saturation (see figure 15).

This undesired non-monotonic behavior of the output conductance becomes intensified when hot-carrier behavior is included. In Mextram this problem is solved by adding an extra collector charge (Chapter 6 [4]).

8 Base resistance

The total base resistance in Vbic95 and Mextram is divided in a constant and a variable part. The extrinsic PNP transistor is connected to the internal node between the two resistors. The base resistance formulation is given in table 6.

In Mextram the variable part of the base resistance is modulated by the term q_b (depletion and diffusion charges) and DC current crowding (see figures 16).

Note that current crowding increases the base resistance when the base current flows

Oct 28, 1996
09:03:30

Comparison Vbic95 and Mextram model

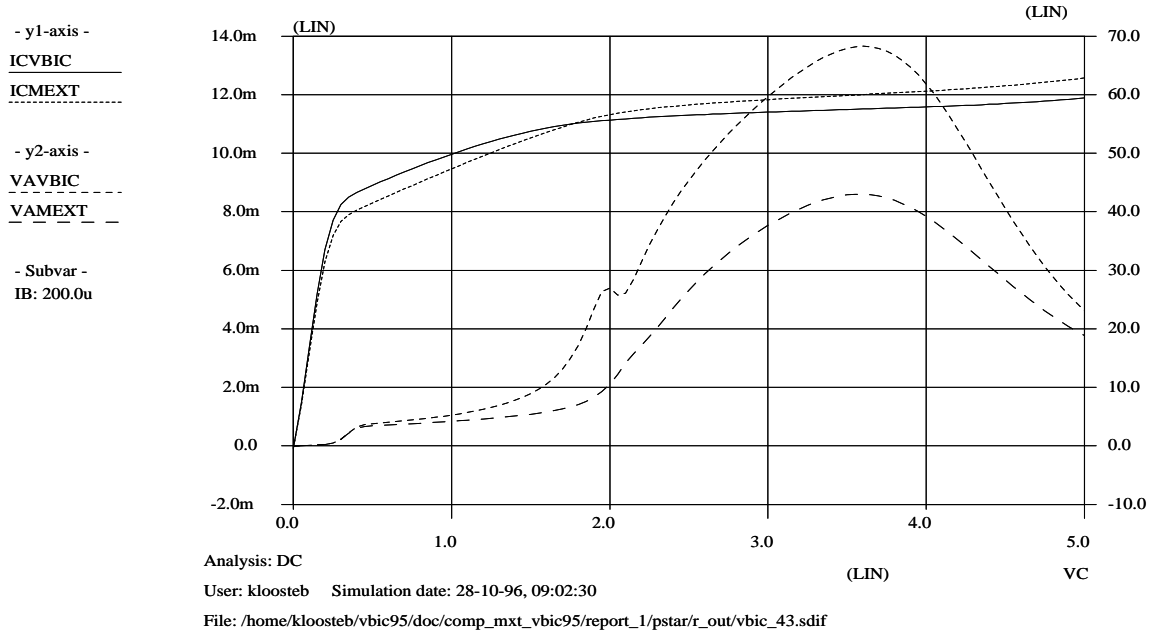


Figure 15: The output conductance in the Vbic95 model may be non-monotonic in the onset to quasi-saturation. This problem is solved in the Mextram model. Velocity saturation is excluded in the simulation. In the figure the collector current and the Early voltage of the Vbic95 model are labeled as ICVBIC (y1-axis) and VAVBIC (y2-axis) whereas the Mextram curves are labeled with ICMEXT and VAMEXT.

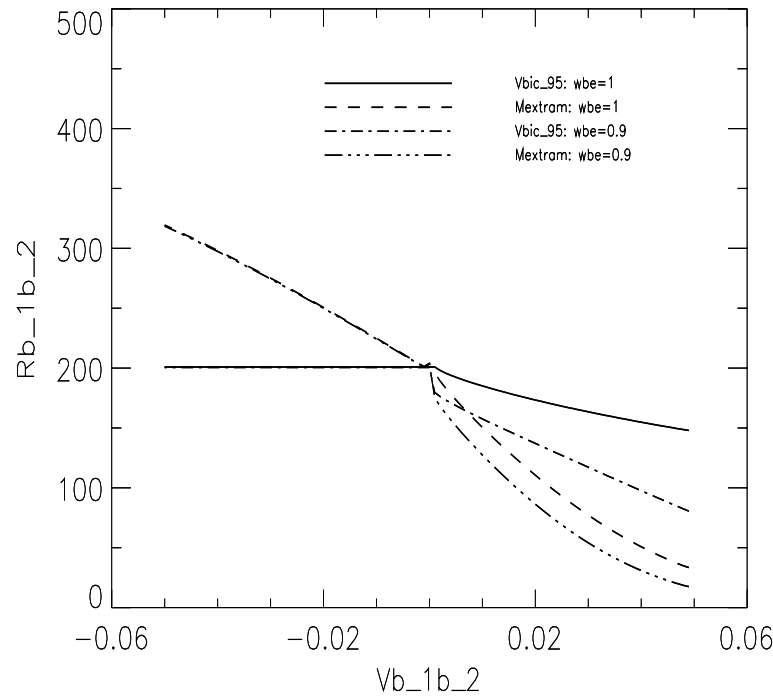


Figure 16: Comparison of the intrinsic base resistance of the Vbic95 and Mextram model. The base resistance parameter value is 250Ω . DC current crowding has a large impact on the base resistance. WBE is the fraction of the base current assigned to the internal b-e node.

in opposite direction. AC current crowding is modelled by an extra capacitance over the variable part of the base resistance. Also in Vbic95 the modulation of the pinched base resistance due to the depletion and base charges is taken into account whereas the base-emitter sidewall current and depletion charge account for DC and AC current crowding. In figures 16 the base resistance is defined as being Vb_1b_2/Ib . The base current Ib is the sum of the current through the base resistance and the current of the base-emitter sidewall junction. The base resistance is plotted for two values of the Vbic95 parameter WBE. For WBE is one there is no sidewall current and the modulation of the base resistance in Vbic95 and Mextram up to moderate base current is mainly due to qb and more or less the same. At these relative small base currents the resistance decreases from 250Ω to about 200Ω . This initial decrease at $Vb_1b_2 \approx 0$ is not shown in figure 16. At higher base current DC current crowding reduces the base resistance considerably in Mextram. When the base current flows in opposite direction during de-charging of the e-b junction the base resistances increases above the nominal parameter value of 250Ω . In this situation the base resistance is constant in Vbic95 and equal to RBI/q_b . For WBE is 0.9 the effective base resistance decreases due to the increase of the base current (see table 2 with $V_{be}^x = V_{be}^i + Vb_1b_2$). For Vbic95 the reduction is relative larger due to the higher initial resistance. However the effective base resistance is still larger then in the Mextram model. In general the presence of the base-emitter sidewall

base-current has a strong impact on the DC current gain and also on the cut-off frequency f_T (see fig. 17). Certainly the influence on the cut-off frequency is not obvious. It is mainly caused by the increase of the AC base current (see fig. 19). In Mextram (see fig. 18) these effects are less severe due to the smaller effective base resistance at high current levels.

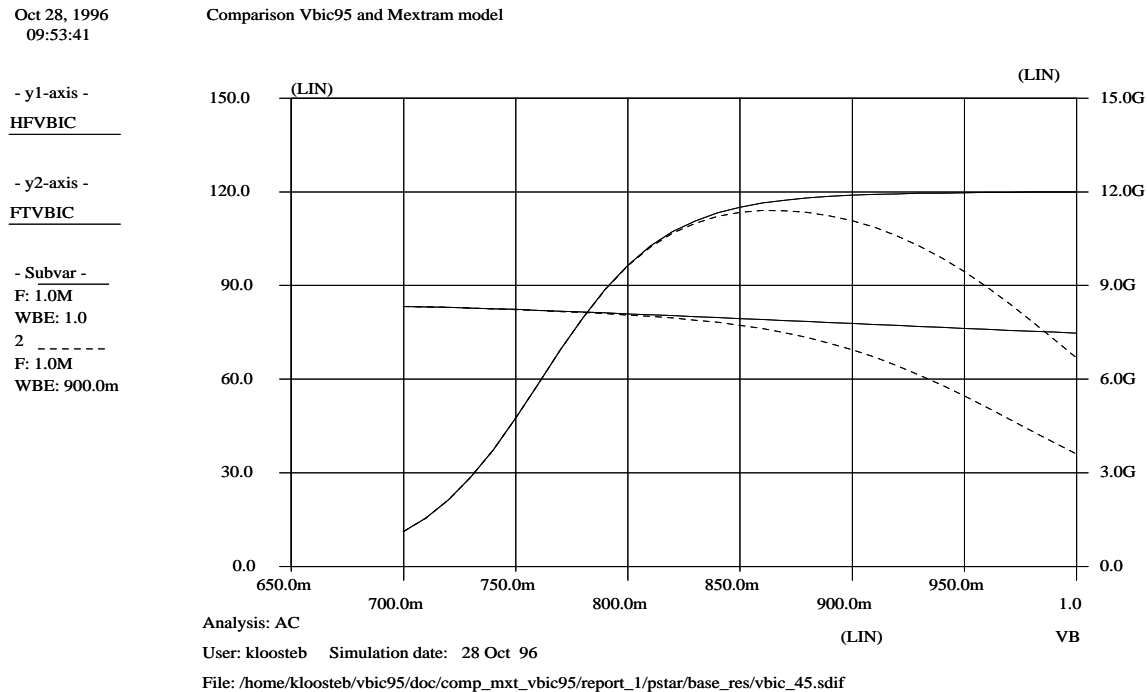


Figure 17: In the figure on the left axis the DC current gain and on the right axis the cut-off frequency is plotted as a function of the base-emitter junction voltage. High injection is excluded in the simulation. The DC gain is labeled as HFVBIC and the cut-off frequency as FTVBIC. The simulation are performed for WBE=1 (no base current sidewall component) and WBE=0.9. The sidewall base current component in Vbic95 may decreases significantly the DC and cut-off frequency.

The base-emitter sidewall capacitance has only minor effects in normal forward mode of operation. In Mextram separate parameters (XI_{bi} , XC_{je}) are used to define the base-emitter sidewall components. In most cases XI_{bi} is much smaller then XC_{je} . It will be clear that the base-emitter sidewall base current has a large impact on the model parameters related to the roll-off of the current gain and cut-off frequency. When we use the same base resistance parameters then these effects are larger in Vbic95 due to the absence of DC/AC current crowding in the base resistance model.

9 Cut-off frequency

The cut-off frequency is the frequency where the AC current gain becomes unity. It can be calculated from AC small signal analysis at a relative low frequency in this

Oct 28, 1996
09:56:14

Comparison Vbic95 and Mextram model

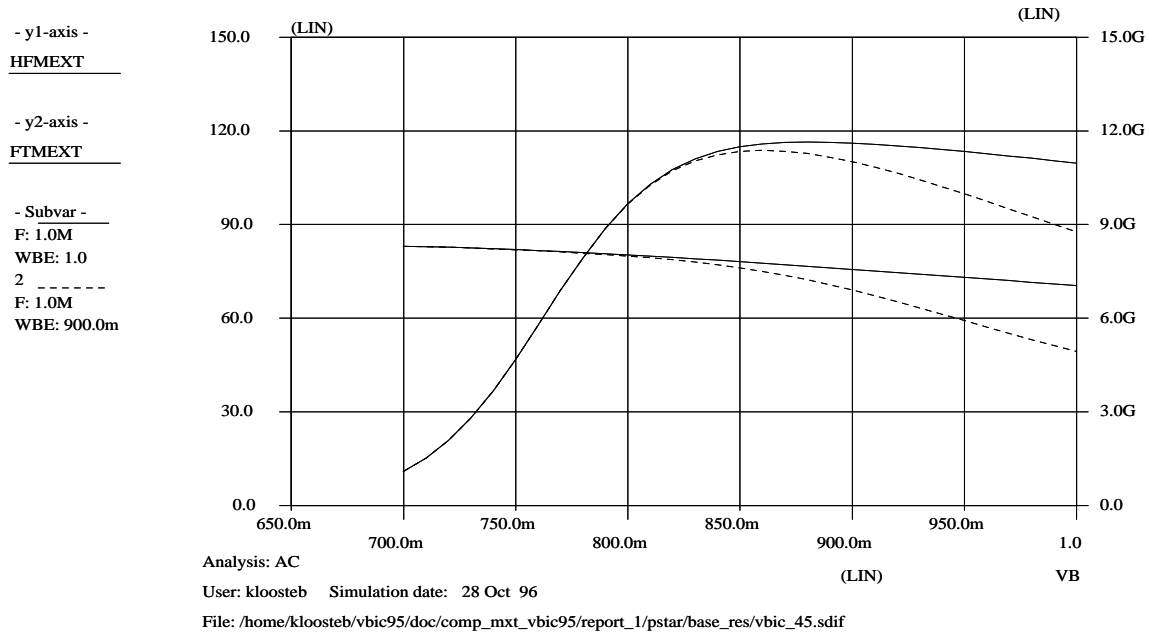


Figure 18: In Mextram the reduction in gain and cutt-off frequency is less severe due to the reduced base resistance caused by current crowding.

way;

$$f_T = \frac{freq}{imag(i_b/i_c)}$$

The maximum value of the cut-off frequency f_T is given by the minimum of the emitter, base and collector transit time. The emitter, base and collector diffusion charges of the Vbic95 and Mextram model are given in table 7.

In Vbic95 the diffusion charge Q_{de} is a function of the forward transit time and is backward compatible with the SGP model. The formulation is extended with the term $(1 + QTF \cdot q_1)$ to include the Early effect of the base transit time. Parameter QTF is the fraction of the total transit time that belongs to the base transit time because only this part is modulated by the base width. The SGP transit time parameters XTF , ITF , VTF and TR can only be used in Vbic95 when we exclude the collector epilayer model. The diffusion charge Q_{dc} is made proportional with the reverse current I_r and the substrate current I_{tf}^p . The contribution of the epilayer charge Q_{epi} to the reverse transit time is proportional with $QCO \cdot GAMM / I_s$ at small base collector voltages. At high base collector voltages ($GAMM \cdot \exp(V_{bc}/V_t) \gg 1$) Q_{epi} becomes proportional with $\exp(V_{bc}/(2 \cdot V_t))$.

In Mextram the emitter, base and collector diffusion charges are defined for each region separately. The base-emitter charge Q_{de} consist of the base charge controlled by the internal b-e junction voltage and the neutral emitter charge. The first term of

Oct 28, 1996
10:01:58

Comparison Vbic95 and Mextram model

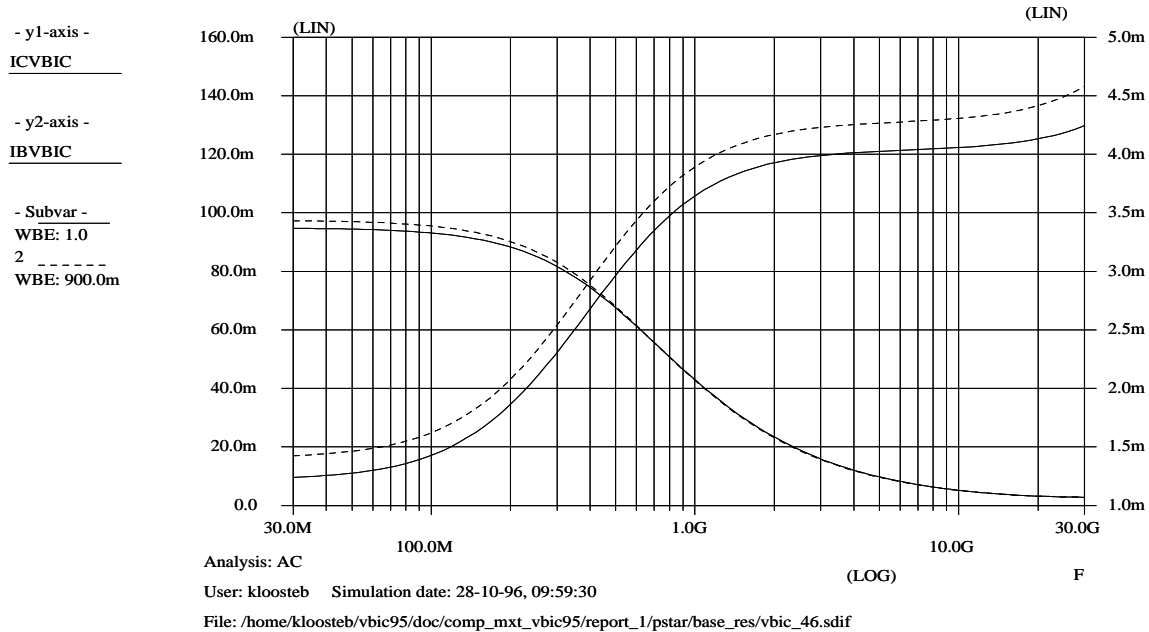


Figure 19: In this figure the AC collector current labeled as ICVBIC is plotted on the right axis while the AC base current is plotted on the left axis denoted by IBVBIC for two values of WBE. The increased base current, due to the b-e sidewall diode, reduces the DC current gain and cut-off frequency f_T ($V_{be} = 0.9V$, $RBX = 50$, $RBI = 250$).

| | Vicb95 | Mextram |
|-----------|---|--|
| Q_{de} | $\tau_{ff} \cdot \frac{I_f}{q_b}$ $\tau_{ff} = \tau_f \cdot (1 + QTF \cdot q_1) \cdot$ $\left\{ 1 + XTF \cdot \left(\frac{I_f}{I_f + ITF} \right)^2 \cdot \right.$ $\left. \exp \left(\frac{V_{bc}^i}{1.44 \cdot VTF} \right) \right\}$ | $q_1 \cdot \frac{Q_{b0}}{I_K} \cdot \frac{I_s}{q_{be}(V_{be}^i)} \cdot \exp \left(\frac{V_{be}^i}{V_t} \right) +$ $Q_{n0} \cdot \left\{ \exp \left(\frac{V_{be}^i}{\tau \cdot V_t} \right) - 1 \right\}$ |
| Q_{dc} | $TR \cdot (I_r + I_{if}^p)$ | $\frac{Q_{b0}}{I_K} \cdot \left\{ q_1 \cdot \frac{I_s}{q_{bc}(V_{bc}^i)} \cdot \exp \left(\frac{V_{bc}^i}{V_t} \right) + \frac{1 - XC_{jc}}{XC_{jc}} \cdot \right.$ $\left((1 - X_{EXT}) \cdot \frac{I_s}{q_{bc}(V_{be}^p)} \cdot \exp \left(\frac{V_{be}^p}{V_t} \right) + \right.$ $\left. \left. X_{EXT} \cdot \frac{I_s}{q_{bc}(V_{be}^{xp})} \cdot \exp \left(\frac{V_{be}^{xp}}{V_t} \right) \right) \right\}$ |
| Q_{epi} | $QCO (K_i + K_x)$ | $I_s \cdot Q_{b0} \cdot \left\{ \frac{\exp(V_{bc}^i/V_t) - \exp(V_{bc}^x/V_t)}{I_{epi}} + \right.$ $\frac{1 - XC_{jc}}{XC_{jc}} \cdot \frac{Rcv}{V_t} \cdot \left((1 - X_{EXT}) \cdot \frac{\exp(V_{be}^p/V_t)}{q_{be}^p(V_{be}^p)} + \right.$ $\left. \left. X_{EXT} \cdot \frac{\exp(V_{be}^{xp}/V_t)}{q_{be}^p(V_{be}^{xp})} \right) \right\}$ |

Table 7: Description of the emitter-base-collector diffusion charges in the Vicb95 and Mextram model. The terms q_{be} , q_{bc} , and q_{be}^p account for high injection effects.

Q_{dc} is the base charge controlled by the internal b-c junction voltage and the second term account for base-collector charge of the extrinsic b-c junction. The scaling with geometry ($XCjc$) is part of the model. Also the total epilayer charge Q_{epi} is divided over three parts being the area under the emitter, the floor area besides the emitter and the sidewall of the b-c junction. Most of the charge component exhibit high injection and the terms $q_{bc}(V)$, $q_{bc}(V)$ and $q_{bc}^p(V)$ account for it. The terms are rather long and therefore omitted in the table. They can be found in [5]. Only the emitter charge model need an additional parameter $Qn0$. The base and collector diffusion charges parameters are extracted from static current characteristics. This implied that these parameters should have a physical value. The reduction in DC gain and cut-off frequency due to base-push out have to be described by the same epilayer parameter set. In most cases we are able to describe the DC gain and cut-off frequency sufficient accurate over a large current and collector voltage range. The presence of a collector epilayer resistance in the Vbic95 model will introduce additional collector transit times and causes base push-out at sufficient high collector currents. It will be difficult to correct the SGP transit time parameters for these effects without doing real parameter extraction. During parameter extraction TR will become small. In many cases I think it will be quite difficult to get with Vbic95 a good description of the f_T when we include the collector epilayer resistance model. This can partly be circumvented by postponing velocity saturation ($V0$ high) and use the knee current IKF to describe the reduction in current gain.

Also the cut-off frequency (same as the Early voltage in figures 15) will not decreases monotonly in the transition to quasi-saturation when the collector transit time ($Cjc \cdot RCI$) becomes a relevant part of the total transit time.

The base and collector diffusion charges (Q_{dc} , Q_{epi} in table 7) of the Vbic95 model are quite simple and does not take into account the differences in doping profile of the active NPN and the parasitic PNP transistor and the different junction areas. In fact Q_{dc} should read $TR^i \cdot I_r + TR^p \cdot I_{tf}^p$ and Q_{epi} should be $QCO^i \cdot K_i + QCO^p \cdot K_x$. Here QCO^i account for the epilayer charge underneath the emitter (important for base-push out in the forward mode of operation) and QCO^p for the epilayer charge of the parasitic PNP transistor (reverse mode of operation). The best work around is to set TR to $TR^i = TF$ and extract QCO from the reverse f_T characteristic and use the SGP transit time parameters to model the f_T curves at high V_{cb} .

10 Temperature scaling rules.

In this section the temperature scaling rules of Vbic95 and Mextram are reviewed. In tables 8, 9 and 10 the scaling rules of corresponding parameters with the same physical meaning are examined. Therefore the tables do not contain the complete set of equations for temperature mapping. From these tables it is convenient to convert the temperature parameters of the Vbic95 and Mextram model. It is not possible to have the same temperature behavior for both models. Therefore choices have to be made, e.g. same temperature dependence of the forward current gain or b-e depletion capacitances. First in tables 8 and 9 the different saturation currents

are compared. The temperature dependence of the collector current I_s becomes the same when $XIS = 3.8 - 1.5 \cdot AB$ and $EA = VGB$. In Vbic95 the substrate current I_{cc}^p has the same temperature dependence as the collector current. In Mextram two additional parameters AS and VGS are used. The temperature dependence of the forward current gain is mainly given by the difference between VGB and VGE and becomes the same for both models when $XII = 3.77$ and $EAIE = VGE$. Now the temperature scaling of the b-e diffusion voltage Vde (see table 9) will be different when $VGB \neq VGE$. The parameters VGB and $EAIE$ are usually determined from the temperature dependence of the collector current and forward current gain and not from the capacitance and diffusion voltage of the b-e junction. The diffusion voltage is mainly given by the lowest doping level near the junction and for the b-e junction this is the doping level of the base. It is therefore not obvious in Vbic95 to make Vde dependent on $EAIE$ being the bandgap of the emitter. For the non-ideal component of the forward base current I_{be}^n we assume that $NEN = 2$ and then $XIN = 4$ and $EANE = VGJ$. The temperature dependence of the reverse base current I_{be}^p depends in Vbic95 on XII and $EAIC$ whereas in Mextram I_{be}^p has the same temperature scaling as the collector current (BRI is temperature independent). For the non-ideal component of the reverse base current I_{be}^{np} we assume that $NCN = 2$ and then $EANC = VGC$ (note that $XIN = 4$ given by component I_{be}^n). The knee current of the intrinsic NPN and extrinsic PNP transistor are temperature independent in Vbic95 whereas in Mextram they depend on parameter AB and AS . AB is determined from the temperature dependence of the pinched base resistance (Rbv) and AS equals to AC in the case the collector plug surround completely the extrinsic base region otherwise $AS = AEPI$.

In general the temperature parameters of the three depletion capacitances are not determined from capacitance measurements. In Mextram VGB is extracted from the temperature dependence of the collector current, VGC is extracted from the collector diffusion voltage (transistor operating in quasi-saturation) and VGS is extracted from the temperature dependence of the substrate current. For Vbic95 $EAIE$ will be extracted from the temperature dependence of the forward current gain, $EAIC$ from the temperature dependence of the reverse current I_{be}^{ip} and $EAIS$ either from the current of the forward biased substrate-collector junction or the substrate-collector depletion capacitance. For the purpose of parameter conversion $EAIE = VGE$, $EAIC = VGC$ and $EAIS = VGS$. The zero junction capacitances Cj have the same temperature dependence in Vbic95 and Mextram. The diffusion voltage may become negative at high temperatures when the parameter value at room temperature is small (< 0.5 Volt). This problem is solved in the Vbic95 model.

The temperature scaling of the series resistances in Vbic95 and Mextram (see table 10) uses the same equations. In Vbic95 the variable and constant part of the collector and base resistance have the same power exponent whereas in Mextram different values are used. Especially the temperature dependence of the lightly doped collector epilayer will be different from the highly doped buried layer. The emitter resistance is temperature independent in the Mextram model. For the purpose of parameter conversion $XRC = AC$, $XRB = AB$ and $XRE = 0$.

| | Vicb95 | Mextram |
|------------|---|--|
| I_s | $I_s^r \cdot \left[\left(\frac{T_k}{T_k^r} \right)^{XIS} \cdot \exp \left\{ EA \cdot \left(\frac{1}{V_t^r} - \frac{1}{V_t} \right) \right\} \right]^{\frac{1}{NEP}}$ | $I_s^r \cdot \left(\frac{T_k}{T_k^r} \right)^{3.8-1.5 \cdot AB} \cdot \exp \left\{ VGB \cdot \left(\frac{1}{V_t^r} - \frac{1}{V_t} \right) \right\}$ |
| I_{be}^i | $I_{be}^{ir} \cdot \left[\left(\frac{T_k}{T_k^r} \right)^{XII} \cdot \exp \left\{ (EAIE) \cdot \left(\frac{1}{V_t^r} - \frac{1}{V_t} \right) \right\} \right]^{\frac{1}{NEI}}$ | $\frac{I_s^r}{B_f^r} \cdot \left(\frac{T_k}{T_k^r} \right)^{3.77} \cdot \exp \left\{ (VGE) \cdot \left(\frac{1}{V_t^r} - \frac{1}{V_t} \right) \right\}$ |
| I_{be}^n | $I_{be}^{nr} \cdot \left[\left(\frac{T_k}{T_k^r} \right)^{XIN} \cdot \exp \left\{ EANE \cdot \left(\frac{1}{V_t^r} - \frac{1}{V_t} \right) \right\} \right]^{\frac{1}{NEI}}$ | $I_{bf}^r \cdot \left(\frac{T_k}{T_k^r} \right)^2 \cdot \exp \left\{ \frac{VGJ}{2} \cdot \left(\frac{1}{V_t^r} - \frac{1}{V_t} \right) \right\}$ |
| I_{cc}^p | $I_s^{pr} \cdot \left[\left(\frac{T_k}{T_k^r} \right)^{XIS} \cdot \exp \left\{ EA \cdot \left(\frac{1}{V_t^r} - \frac{1}{V_t} \right) \right\} \right]^{\frac{1}{NEP}}$ | $I_{ss}^r \cdot \left(\frac{T_k}{T_k^r} \right)^{3.5+AS} \cdot \exp \left\{ VGS \cdot \left(\frac{1}{V_t^r} - \frac{1}{V_t} \right) \right\}$ |
| I_{be}^p | $I_{be}^{ipr} \cdot \left[\left(\frac{T_k}{T_k^r} \right)^{XII} \cdot \exp \left\{ EAIC \cdot \left(\frac{1}{V_t^r} - \frac{1}{V_t} \right) \right\} \right]^{\frac{1}{NEI}}$ | $\frac{I_s^r}{BRI} \cdot \left(\frac{T_k}{T_k^r} \right)^{3.8-1.5 \cdot AB} \cdot \exp \left\{ VGB \cdot \left(\frac{1}{V_t^r} - \frac{1}{V_t} \right) \right\}$ |

Table 8: Comparison of the temperature scaling rules. Only parameters with the same physical meaning are treated.

| | Vicb95 | Mextram |
|---------------|--|---|
| I_{be}^{np} | $I_{be}^{np^r} \cdot \left[\left(\frac{T_k}{T_k^r} \right)^{XIN} \right]$ $\exp \left\{ EANC \cdot \left(\frac{1}{V_t^r} - \frac{1}{V_t} \right) \right\}^{\frac{1}{NCN}}$ | $Ib_r^r \cdot \left(\frac{T_k}{T_k^r} \right)^2$ $\exp \left\{ \frac{VGC}{2} \cdot \left(\frac{1}{V_t^r} - \frac{1}{V_t} \right) \right\}$ |
| IKF | IKF^r | $IK^r \cdot \left(\frac{T_k}{T_k^r} \right)^{1-AB}$ |
| IKP | IKP^r | $IKS^r \cdot \left(\frac{T_k}{T_k^r} \right)^{1-AS}$ |
| Vde | $-3 \cdot V_t \cdot \ln \left(\frac{T_k}{T_k^r} \right) + PE^r \cdot \left(\frac{T_k}{T_k^r} \right) +$ $\left(1 - \left(\frac{T_k}{T_k^r} \right) \right) \cdot EAIE$ | $-3 \cdot V_t \cdot \ln \left(\frac{T_k}{T_k^r} \right) + Vde^r \cdot \left(\frac{T_k}{T_k^r} \right) +$ $\left(1 - \left(\frac{T_k}{T_k^r} \right) \right) \cdot VGB$ |
| Vdc | $-3 \cdot V_t \cdot \ln \left(\frac{T_k}{T_k^r} \right) + PC^r \cdot \left(\frac{T_k}{T_k^r} \right) +$ $\left(1 - \left(\frac{T_k}{T_k^r} \right) \right) \cdot EAIC$ | $-3 \cdot V_t \cdot \ln \left(\frac{T_k}{T_k^r} \right) + Vdc^r \cdot \left(\frac{T_k}{T_k^r} \right) +$ $\left(1 - \left(\frac{T_k}{T_k^r} \right) \right) \cdot VGC$ |
| Vds | $-3 \cdot V_t \cdot \ln \left(\frac{T_k}{T_k^r} \right) + PS^r \cdot \left(\frac{T_k}{T_k^r} \right) +$ $\left(1 - \left(\frac{T_k}{T_k^r} \right) \right) \cdot EAIS$ | $-3 \cdot V_t \cdot \ln \left(\frac{T_k}{T_k^r} \right) + Vds^r \cdot \left(\frac{T_k}{T_k^r} \right) +$ $\left(1 - \left(\frac{T_k}{T_k^r} \right) \right) \cdot VGS$ |
| Cj | $Cj^r \cdot \left(\frac{P^r}{P} \right)^M$ | $Cj^r \cdot \left(\frac{Vd^r}{Vd} \right)^P$ |

Table 9: Continued table

| | Vicb95 | Mextram |
|----------|--|--|
| R_{cc} | $RCX^r \cdot \left(\frac{T_k}{T_k^r}\right)^{XRC}$ | $R_{cc}^r \cdot \left(\frac{T_k}{T_k^r}\right)^{AC}$ |
| R_{cv} | $RCI^r \cdot \left(\frac{T_k}{T_k^r}\right)^{XRC}$ | $R_{cv}^r \cdot \left(\frac{T_k}{T_k^r}\right)^{AEPI}$ |
| R_{bc} | $RBX^r \cdot \left(\frac{T_k}{T_k^r}\right)^{XRB}$ | $R_{bc}^r \cdot \left(\frac{T_k}{T_k^r}\right)^{AEX}$ |
| R_{bv} | $RBI^r \cdot \left(\frac{T_k}{T_k^r}\right)^{XRB}$ | $R_{bv}^r \cdot \left(\frac{T_k}{T_k^r}\right)^{AB}$ |
| R_e | $RE^r \cdot \left(\frac{T_k}{T_k^r}\right)^{XRE}$ | Re^r |
| R_s | $RS^r \cdot \left(\frac{T_k}{T_k^r}\right)^{XRS}$ | — |
| R_{bp} | $RBP^r \cdot \left(\frac{T_k}{T_k^r}\right)^{XRC}$ | — |

Table 10: *Temperature scaling of the series resistances*

11 Conversion of Mextram to Vbic95 parameters.

In this section the conversion of Mextram to Vbic95 parameters will be treated. In Vbic95 some of the parameters intended to describe the reverse mode of operation are also used in quasi-saturation. The first claim in the conversion is to simulate the forward characteristics including quasi-saturation as close as possible to the Mextram characteristics.

The parameters of the three depletion capacitances can be converted straight forward. Be aware that the diffusion voltage in Vbic95 has the same name as the grading coefficient in Mextram.

$$\begin{aligned}
 CJE &= Cje \\
 PE &= Vde \\
 ME &= Pe \\
 WBE &= 1 - XCje \\
 AJE &= 0.01 \\
 FC &= 0.9 \\
 CBEO &= 0
 \end{aligned}$$

$$\begin{aligned}
 CJC &= XCjc \cdot Cjc \\
 CJEP &= (1 - XCjc) Cjc \\
 PC &= Vdc \\
 MC &= (1 - Xp) \cdot Pc \\
 AJC &= 0.01 \\
 CBCO &= = 0
 \end{aligned}$$

$$\begin{aligned}
 CJCP &= Cjs \\
 PS &= Vds \\
 MS &= Ps \\
 AJS &= 0.01
 \end{aligned}$$

The forward and reverse Early voltages has to be computed in this way;

$$\begin{aligned}
 VEF &= \frac{Qb0}{XCjc \cdot Cjc} \\
 VER &= \frac{Qb0}{(1 - XCje) \cdot Cje}
 \end{aligned}$$

The parameters of the forward and reverse Gummel plot up to medium current levels can be easily converted. The most accurate and robust way to determine the parameters of the non-ideal base components is to calculate two points and use these

data points to calculate the intersect $IBEN$ and the slope NEN . Suitable choices for the two points at room temperature are 0.5 and 0.7 Volt. The procedure then becomes;

$$\begin{aligned}
 V_1 &= 0.5 \\
 V_2 &= 0.7 \\
 Ib_1 &= Ib_f \left\{ \frac{\exp\left(\frac{V_1}{V_t}\right) - 1}{\exp\left(\frac{V_1}{2 \cdot V_t}\right) + \exp\left(\frac{V_{LRF}}{2 \cdot V_t}\right)} \right\} \\
 Ib_2 &= Ib_f \left\{ \frac{\exp\left(\frac{V_2}{V_t}\right) - 1}{\exp\left(\frac{V_2}{2 \cdot V_t}\right) + \exp\left(\frac{V_{LRF}}{2 \cdot V_t}\right)} \right\} \\
 NEN &= \frac{V_2 - V_1}{V_t \cdot \ln\left(\frac{Ib_1}{Ib_2}\right)} \\
 IBEN &= \frac{Ib_1}{\exp\left(\frac{V_1}{NEN \cdot V_t}\right)}
 \end{aligned} \tag{2}$$

In the same way $IBENP$ and NCN can be calculated from the Mextram parameters Ibr and VLR (see table 4). The other parameters of the Gummel plots are listed below. Note that the reverse base current $IBCI$ and $IBCN$ of the intrinsic NPN transistor are zero.

$$\begin{aligned}
 IS &= I_s \\
 NF &= 1 \\
 NR &= 1 \\
 IKF &= IK \\
 IKR &= IK \\
 \\
 IBEI &= I_s/Bf \\
 NEI &= 1 \\
 IBCI &= 0 \\
 IBCN &= 0 \\
 \\
 ISP &= I_{ss} \\
 NFP &= 1 \\
 WSP &= 1 \\
 IKP &= \frac{I_{ss}}{I_s} \cdot IKS
 \end{aligned}$$

$$\begin{aligned}
IBEIP &= I_s/BRI \\
NCI &= 1 \\
IBCIP &= I_{ss} \\
NCIP &= 1 \\
IBCNP &= 0 \\
NCNP &= 2
\end{aligned}$$

The series resistances of the base, emitter and constant part of the collector are the same. The Mextram model does not have base resistances for the PNP transistor and substrate series resistance.

$$\begin{aligned}
RBX &= Rbc \\
RBI &= Rbv \\
RE &= Re \\
RCX &= Rcc \\
RCI &= Rcv \\
GAMM &= 4 \cdot \exp(-Vdc/Vt) \\
VO &> Ihc \cdot Rcv \\
HRCF &= \frac{SCRcv}{2 \cdot Rcv} \\
RS &= .. \\
RBP &= ..
\end{aligned}$$

The description of velocity saturation in Vbic95 is not correct and therefore it has to be postponed to higher current levels. This can be achieved by making VO sufficient high. In this case the description of the gain at high current levels may be improved by lowering the forward knee current IKF .

The avalanche model in Vbic95 and Mextram is the same for transistors with relative thick epilayers operating at small collector currents. The computed avalanche current is too large in Vbic95 when the depletion layer extend into the buried layer. The parameter conversion becomes;

$$\begin{aligned}
AVC1 &= \frac{A_n}{B_n} \cdot (1 - (1 - Xp) \cdot Pc) \\
AVC2 &= AVL \cdot \frac{1 - (1 - Xp) \cdot Pc}{Vdc^{(1-Xp) \cdot Pc}}
\end{aligned}$$

with $A_n = 7.03 \cdot 10^5$ and $B_n = 1.23 \cdot 10^6$.

The diffusion charge related parameters are difficult to convert. In the SGP model the transit time parameters XTF , ITF and VTF are used to describe the degradation of the cut-off frequency in quasi-saturation. In the Vbic95 model the presence of the collector resistance RCI now accounts for the reduction in DC and AC gain.

The behavior of the cut-off frequency in quasi-saturation will depend strongly on the transition voltage for velocity saturation VO . This parameter can be used to tune the fT characteristics in quasi-saturation. This procedure can only be carried out by doing real parameter extraction. A first order parameter conversion is;

$$\begin{aligned}
 TF &= \left(1 + \frac{0.7}{VEF}\right) \cdot \left(\frac{Qb0}{IK} + Taune\right) \\
 QTF &= \frac{Qb0}{Qb0 + IK \cdot Taune} \\
 XTF &= 1 \\
 VTF &= Ihc \cdot Rcv \\
 ITF &> Ihc \\
 TR &= \frac{Qb0}{IK} \\
 QCO &= \frac{Qb0 \cdot Rcv \cdot Is}{4 \cdot XCjc \cdot \exp(Vdc/Vt)}
 \end{aligned}$$

Parameter ITF have to be larger then Ihc because the resistance RCI accounts for the decrease of the cut-off frequency at medium collector currents.

The temperature scaling rule parameters have to be converted as follows;

$$\begin{aligned}
 EA &= VGB \\
 EAIE &= VGE \\
 EAIC &= VGC \\
 EAIS &= VGS \\
 EANE &= VGJ \\
 EANC &= VGC \\
 EANS &= VGS \\
 XIS &= 3.8 - 1.5 \cdot AB \\
 XII &= 3.77 \\
 XIN &= 4 \\
 TNF &= 0 \\
 TAVC &= 7.2 \cdot 10^{-4} \\
 XRE &= 0 \\
 XRB &= AB \\
 XRC &= AC \\
 XRS &= 0 \\
 XVO &= AEPI
 \end{aligned}$$

12 Conclusions

Recently a new bipolar transistor model Vbic95 has been introduced for bipolar modelling and characterization. The Vbic95 model is in many aspect compatible with the current standard, the Spice Gummel Poon (SGP) model. Compatibility with the Spice Gummel Poon model is an advantage because parameters can simply be converted from the SGP model to the Vbic95 model. However when one of the new features of the Vbic95 model is used (e.g. epilayer resistance) most of the high current SGP parameters will change dramatically and can only be obtained via parameter extraction.

The main improvements of the Vbic95 model over the SGP model are the explicit modelling of the parasitic PNP transistor, bias dependent Early voltages, modelling of the epilayer resistance (base push-out), avalanche multiplication, and the extensive temperature mapping. Also self heating of the transistor can be taken into account. The intrinsic NPN transistor and the parasitic PNP transistor are basically SGP models with proven simple equations.

The description of the variable epilayer resistance is based on the Kull model [2] and extended with velocity saturation. The combined effect of base push-out and velocity saturation is badly modelled and makes the Vbic95 unsuitable to describe accurately the degradation of current gain and cut-off frequency in quasi-saturation. There are many parameters in Vbic95 to describe quasi-saturation. These are the SGP parameters XTF , ITF and VTF , the new parameter QTF , the epilayer parameters RCI , $HRCF$, VO , $GAMM$, and QCO , the reverse transit time TR and the reverse base current parameters $IBCI$ and $IBCN$. All these parameters effect the collector current and the cut-off frequency in quasi-saturation more or less and therefore they becomes strongly correlated. Therefore parameter extraction in this operating region will be quite cumbersome.

In this report the Vbic95 model release 1.1.4 is compared with the Mextram model. The Mextram model equations are more complicated whereas the number of model parameters is minimized. In Vbic95 the model equations are relative simple with many parameters. Therefore the understanding of the Mextram model is more difficult especially the interaction between the DC and AC part.

The main difference in the equivalent circuit of both models is the single parasitic PNP device in Vbic95 in contrast to a bottom and sidewall PNP in Mextram. The sidewall PNP will improve the modeling of the reverse Gummel plot and the on resistance of the output characteristic. The Vbic95 model possess substrate series resistance and this improves the admittance Y_{22} at high frequencies. The Vbic95 model has besides the electrical equivalent network also a thermal network and an excess phase network.

In Mextram the base-collector depletion capacitance takes into account the finite

thickness of the epilayer and collector current modulation. In Vbic95 two capacitance parameters are there to define the total base-collector depletion capacitance being $CJC + CJEP$. This is inconvenient during parameters extraction and may be confusing with the SGP parameter set in which CJC account for the total b-c capacitance. Moreover parameter $CJCP$ is the collector-substrate capacitance. The description of the output resistance (Early voltage) up to medium collector currents is the same. At high collector currents the behavior of the output resistance may be quite different due to the bad modelling of velocity saturation in Vbic95.

Avalanche multiplication determines mainly the output resistance at higher collector voltages. The Mextram the avalanche model takes into account the decrease of the maximum electric field (and therefore avalanche multiplication) in the epilayer with collector current and the influence of current spreading. In Vbic95 avalanche multiplication is coupled to the internal base-collector junction voltage V_{bc}^i . This internal collector voltage decreases with current when a epilayer resistance is present and therefore also avalanche multiplication decreases with current and becomes always zero in quasi-saturation. At sufficient high collector current the maximum electric field resides at the collector buried layer and starts to increase with collector current resulting in a negative output resistance. The description of this behavior is optional in the Mextram model.

Each current component of the NPN and PNP transistor in Vbic95 has a non-ideality factor. In most cases this factor has to be one, otherwise it will affect many other parameters. The description of the forward and reverse current gain is more or less the same if we set the non-ideality factor of the collector and substrate current to one and the slope of the non-ideal base currents to two.

In Vbic95 and Mextram the pinched base resistance is modulated by the base width and the base diffusion charge. In addition the Mextram model account for DC and AC current crowding. Therefore the voltage drop over the pinched base resistance in Vbic95 is higher and the sidewall b-e junction current decreases more the forward current gain and cut-off frequency as in the Mextram model. In Vbic95 there is only one parameter to separate the b-e depletion capacitance and base current in a bottom and sidewall component whereas in the Mextram model each component has its own parameter.

The Mextram and Vbic95 has extensive temperature scaling in comparison with the SGP model. In Vbic95 the substrate and collector current has the same temperature scaling parameters whereas in Mextram two different activation energies may be specified. In Vbic95 the b-e diffusion voltage depends on the activation energy of the emitter whereas in Mextram it depends on the activation energy of the base which is more likely. In Vbic95 the pinched base and constant part of the base resistance has the same temperature dependence and the same holds for the collector epilayer resistance and constant part of the collector resistance. In Mextram different temperature scaling parameters may be specified. The emitter resistance is temperature

independent in the Mextram model in contrast to Vbic95.

In Vbic95 the $1/f$ noise may be not ideal ($1/f^{BFN}$) whereas in Mextram the non-ideal and ideal forward base current have its own bias dependency. In Vbic95 shot noise is specified for the substrate current and thermal noise for the epilayer resistance. They are omitted in the Mextram model.

At this moment we can not compare the computational efficiency of both models. Then both models have to be implemented in the same circuit simulator in more or less identical way using the same algorithm for convergency and time step control. My expectation is that the Mextram model will take more computation time to do one model evaluation. The overall computation time will depend strongly on the convergency behavior. The convergency behavior of the Mextram model is good. The convergency behavior of the Vbic95 model will be the same at low and medium current and voltage levels. At high current levels the convergency of the Vbic95 model may be hampered due to the limited collector current caused by the unphysical epilayer model.

To conclude the Vbic95 is at the moment not suitable to replace the Mextram model. The main deficiency is the velocity saturated behavior of the collector epilayer current in combination with base push-out. Monotony of the output conductance and cut-off frequency is not guaranteed when an epilayer resistance is present. The new Vbic95 features (e.g. epilayer resistance) can not be added to the SGP model without repeating parameter extraction. Moreover there are many minor differences in model definitions and its impact on the transistor characteristics can only be examined for individual devices.

A Appendix

```

title: Comparison Vbic95 and Mextram model ;
change;
    dcatr_active = false ;
end;
numform: 7, fix, scientific ;

model: vbic(c,b,e,s) is, bf, wbe, iben, nen,
    br, ibenp, ncn,
    isp, ikp, wsp, av1, av2,
    rbc, rbv, rcc, re, rs, rbp,
    ver, vef , ikf, ikr,
    rcv, vdc , ihc, scrcv, gamm,
    cje, vde, pe , fc , a,
    cjc, pc, xcjc,
    cjs, vds, ps ,
    tauf, qtf, xtf, itf, vtf , qco, taur ,
    xrb, xrc, ea, eaie, eaic, eais, eane, eanc,
    xis, xii, xin, tnf, tav,tref;

c: junction voltages ;
vbei = vn(b2)-vn(e1);
vbex = vn(b1)-vn(e1);
vbci = vn(b2)-vn(c2);
vbcw = vn(b2)-vn(c1);
vbep = vn(b1)-vn(c3);
vbcp = vn(s1)-vn(c3);
vepi = vn(c1)-vn(c2);
vscw = vn(s1)-vn(c3);

gmin=1.e-13;

c: temperature mapping;
vtr  = 1.380662d-23*(tref+2.731500d+02)/1.602189d-19 ;
vt   = 1.380662d-23*(temp+2.731500d+02)/1.602189d-19 ;
rt   = (temp+2.731500d+02)/(tref+2.731500d+02);
ti   = (1/vtr-1/vt);

rcx  = rcc*rt**xrc ;
rci  = rcv*rt**xrc ;
rbx  = rbc*rt**xrb ;
rbi  = rbv*rt**xrb ;

ist  = is*rt**xis*exp(ea*ti) ;

```

```

ispt = isp*rt**xis*exp(ea*ti) ;
ibeit = is/bf*rt**xii*exp(eaie*ti) ;
ibent = iben*(rt**xin*exp(eane*ti))**(1/nen) ;
ibeipt= is/br*rt**xii*exp(eaic*ti) ;
ibenpt= ibenp*(rt**xin*exp(eanc*ti))**(1/ncn) ;

```

```

vdet = vde*rt+(1-rt)*eaie-3*vt*ln(rt);
vdct = vdc*rt+(1-rt)*eaic-3*vt*ln(rt);
vdst = vds*rt+(1-rt)*eais-3*vt*ln(rt);
cjet = cje*(vde/vdet)**pe ;
cjct = cjc*(vdc/vdct)**pc ;
cjst = cjs*(vds/vdst)**ps ;

```

```

gammt = gamm*rt**xis*exp(ea*ti) ;
av2t = av2*(1+tav*(temp-tref));

```

c: vtc;

```

cdv0 = - vdct * fc ;
cmv0 = sqrt ( cdv0 * cdv0 + a ) ;
cvl0 = 0.5 * ( cdv0 - cmv0 ) + vdct * fc ;
cxq0 = -vdct * ( 1.0 - cvl0 / vdct ) ** ( 1.0 - pc ) / ( 1.0 - pc ) ;
cdv = vbci - vdct * fc ;
cmv = sqrt ( cdv * cdv + a ) ;
cvl = 0.5 * ( cdv - cmv ) + vdct * fc ;
cdq = ( 1.0 - cvl / vdct ) ** ( - pc ) ;
cqj = - vdct * ( 1.0 - cvl / vdct ) * cdq / ( 1.0 - pc ) - cxq0 ;
cxx = ( 1.0 - fc ) ** ( - pc ) ;
vtc = cqj + cxx * ( vbci - cvl + cvl0 ) ;

```

c: vtcx;

```

cdvx = vbep - vdct * fc ;
cmvx = sqrt ( cdvx * cdvx + a ) ;
cvlx = 0.5 * ( cdvx - cmvx ) + vdct * fc ;
cdqx = ( 1.0 - cvlx / vdct ) ** ( - pc ) ;
cqjx = - vdct * ( 1.0 - cvlx / vdct ) * cdqx / ( 1.0 - pc ) - cxq0 ;
vtcx = cqjx + cxx * ( vbep - cvlx + cvl0 ) ;

```

c: vte;

```

edv0 = - vdet * fc ;
emv0 = sqrt ( edv0 * edv0 + a ) ;
evl0 = 0.5 * ( edv0 - emv0 ) + vdet * fc ;
exq0 = -vdet * ( 1.0 - evl0 / vdet ) ** ( 1.0 - pe ) / ( 1.0 - pe ) ;
edv = vbei - vdet * fc ;
emv = sqrt ( edv * edv + a ) ;
evl = 0.5 * ( edv - emv ) + vdet * fc ;

```

```

    edq = ( 1.0 - evl / vdet ) ** ( - pe ) ;
    eqj = - vdet * ( 1.0 - evl / vdet ) * edq / ( 1.0 - pe ) - exq0 ;
    exx = ( 1.0 - fc ) ** ( - pe ) ;
    vte = eqj + exx * ( vbei - evl + evl0 ) ;

c: vtex;
    edvx = vbex - vdet * fc ;
    emvx = sqrt ( edvx * edvx + a ) ;
    evlx = 0.5 * ( edvx - emvx ) + vdet * fc ;
    edqx = ( 1.0 - evlx / vdet ) ** ( - pe ) ;
    eqjx = - vdet * ( 1.0 - evlx / vdet ) * edqx / ( 1.0 - pe ) - exq0 ;
    vtex = eqjx + exx * ( vbex - evlx + evl0 ) ;

c: vts;
    sdv0 = - vdst * fc ;
    smv0 = sqrt ( sdv0 * sdv0 + a ) ;
    svl0 = 0.5 * ( sdv0 - smv0 ) + vdst * fc ;
    sxq0 = -vdst * ( 1.0 - svl0 / vdst ) ** ( 1.0 - ps ) / ( 1.0 - ps ) ;
    sdv = vscw - vdst * fc ;
    smv = sqrt ( sdv * sdv + a ) ;
    svl = 0.5 * ( sdv - smv ) + vdst * fc ;
    sdq = ( 1.0 - svl / vdst ) ** ( - ps ) ;
    sqj = - vdst * ( 1.0 - svl / vdst ) * sdq / ( 1.0 - ps ) - sxq0 ;
    sxx = ( 1.0 - fc ) ** ( - ps ) ;
    vts = sqj + sxx * ( vscw - svl + svl0 ) ;

c: intrinsic npn ;
    if = ist*(exp(vbei/vt)-1);
    ir = ist*(exp(vbci/vt)-1);
    xq1 = 1+vte/ver+vte/vef;
    xq2 = if/ikf+ir/ikr;
    qb = 0.5*(xq1+sqrt(xq1*xq1+4*xq2)) ;
    j_in (c2,e1) i=(if-ir)/qb;
    j_ibf(b2,e1) i=wbe*ibeit*(exp(v/vt)-1)+ibent*(exp(v/(nen*vt))-1)+v*gmin;
c: charges ;
    tf = tauf*(1+qtf*xq1)*(1+xtf*(if/(if+itf))**2*exp(vbci/(1.44*vtf)));
    c_ei(b2,e1) q=wbe*vte*cjet+tf*if/qb;
    c_ci(b2,c2) q=vte*xcjc*cjct+taur*ir+qco*k0;
    c_cx(b2,c1) q=qco*kw;

c: base-emitter sidewall ;
    j_ex(b1,e1) i=(1-wbe)*ibeit*(exp(v/vt)-1);
    c_ex(b1,e1) q=(1-wbe)*vtex*cjet;

c: extrinsic pnp ;

```

```

ifp = ispt*(wsp*(exp(vbep/vt)-1)+(1-wsp)*(exp(vbci/vt)-1));
irp = ispt*(exp(vbcp/vt)-1);
xq2p = ifp/ikp;
qbp = 0.5*(1+sqrt(1+4*xq2p)) ;
j_iccp(b1,s1) i=(ifp-irp)/qbp;
j_ibep(b1,c3) i=ibeipt*(exp(v/vt)-1)+ibenpt*(exp(v/(ncn*vt))-1)+v*gmin;
j_ibcp(s1,c3) i=irp;
c_cbep(b1,c3) q=vtcx*(1-xcjc)*cjct+taur*ifp;
c_cbc(s1,c3) q=vts*cjst;

c: resistances ;
r_bc(b,b1) rbx ;
r_bv(b1,b2) i=v*qb/rbi;
r_bp(c1,c3) i=v*qbp/rbp;
r_e(e,e1) re ;
r_c(c,c1) rcx ;
r_s(s,s1) rs ;

c: epilayer model ;
k0 = sqrt(1+gammt*exp(vbci/vt));
kw = sqrt(1+gammt*exp(vbcw/vt));
ec = vt*(k0-kw-ln((k0+1)/(kw+1)));
iepio = (ec+vepi)/rci ;
ih = ihc+sqrt(vepi*vepi+0.01)/scrcv ;
iepi = iepio/sqrt(1+(iepio/ih)**2) ;
r_epic(c1,c2) i = iepi;

c: avalanche model;
adv=vdct-vbci;
asdv=sqrt(adv*adv+0.01d0);
avl=0.5d0*(asdv+adv);
avlm=avl**(pc-1.0d0);
aev=exp(-av2t*avlm);
am=av1*avl*aev;
j_avl(c2,b2) i=am*(if-ir)/qb;

dcapprox;
v(b1,e1)=0.5 ;
v(b1,e1)=0.5 ;
v(b2,c2)=0.5 ;
v(b2,c1)=0.5 ;
v(b1,c3)=0.5 ;
end;
end;

```

```

circuit;
tref= 25;
wepi = 0.5e-4; nepi=1.e17; le=0.5e-4; we=10.e-4; tanl=1; tanh=2;
tk   = tref+2.7315e+02; vt=1.380662e-23*tk/1.602189e-19;
qel  = 1.602e-19; eps=1.036e-12; vlim=8.e6;
cni  = 3.87e16*tk**1.5*exp(-7014/tk);
mu   = 92+(1360-92)/(1+(nepi/1.3e17)**0.91);
sfl  = tanl*wepi*(1/le+1/we);
sfh  = 0.667*tanh*wepi*(1/le+1/we);
vdc  = vt*ln(nepi*nepi/(cni*cni));
ihc  = le*we*qel*nepi*vlim*(1+sfl);
rcv  = wepi/(le*we*qel*nepi*mu)/(1+sfl) ;
scrcv= wepi*wepi/(2*eps*vlim*le*we)/(1+sfh);

is   = 1.e-17 ; bf = 100; xibi=0; br = 20; ik=0.05;
ibf  = 1.e-15; vlf =0.4; ibr=1.e-15; vlr=0.4;
rbc  = 50; rbv=250; rcc = 10; re=2; rsub=10; rbp=rcc; xext=0.5;
ver  = 5 ; vef = 25; qbo=(1-xcje)*cje*ver; xcjc=qbo/(cjc*vef);
iss  = 5.e-18; iks= 1.e-5; avl=25; an=7.03e5; bn=1.23d6;
cje  = 3.e-7*le*we+5.e-12*2*(le+we);
vde  =0.9; pe=0.4 ; xcje=5.e-12*2*(le+we)/cje ;
cjc  = 10f; pc =0.4; xp=0.001; mc=0.3;
cjs  = 20f; vds =0.6; ps =0.3; taune=5e-12; mtau=1;
vge  =1.18; vgb=1.206; vgc=1.15; vgj=1.1; vi=0.04; na=5.e17;
er=0.0; ab=1.0; aepi=2.2; aex=0.5; ac=0.5; vgs=1.206; as=ac;

type: 'test' is=is, bf=bf, wbe=1-xcje, iben=ibf, nen=2,
      br=br, ibenp=ibr, ncn=2, ikf=ik,
      ikr=ik, av2=avl*(1-pc)/(vdc**pc),
      isp=iss, ikp=iss*iks/is, wsp=1, av1=an/(bn*(1-pc)),
      rbc=rbc, rbv=rbv, rcc=rcc, re=re, rs=rsub, rbp=rbp, ver=ver,
      vef=vef, rcv=rcv, vdc=vdc, ihc=3*ihc, scrcv=scrcv,
      gamm=4.*exp(-vdc/vt),
      cje=cje, vde=vde, pe=pe, fc=0.9, a=0.01,
      cjc=cjc, pc=pc, xcjc=xcjc, cjs=cjs, vds=vds, ps=ps,
      tauf=(1+0.7/ver)*(qbo/ik+taune), qtf=qbo/(qbo+ik*taune),
      xtf=1.0, vtf=ihc*rcv, itf=2*ihc, taur=qbo/ik,
      qco=rcv*is*qbo/(4.*exp(-vdc/vt)*vt*xcjc),
      xrb=aex, xrc=ac, ea=vgb, eaie=vge,
      eaic=vgb, eais=vgs, eane=vgj, eanc=vgc,
      xis=3.8-1.5*ab, xii=3.77, xin=2, tnf=0, tav= 7.2e-4, tref=tref;

type: 'testm' level= 503, is=is, bf=bf, bri=br, rbc=rbc, xibi=xibi,
      rcc=rcc, re=re, rbv=rbv, ik=ik, ibr=ibr, ibf=ibf, vlf=vlf,
      vlr=vlr, qbo =qbo, xcjc=xcjc, iss=iss, iks=iks, avl=avl,

```

```

rcv=rcv, vdc=vdc, ihc = ihc, scrcv=scrcv, eta=3, xext=xext,
cje=cje, vde=vde, pe=pe, xcje=xcje,
cjc=cjc, pc=pc/(1-xp), mc=mc, xp=xp, sfh=sfh,
cjs=cjs, vds=vds, ps=ps, taune=taune, mtau=mtau, tref=tref,
vge=vge, vgb=vgb, vgc=vgc, vgj=vgj, vi=vi, na=na, er=er, ab=ab,
aepi=aepi,aex=aex, ac=ac,as=as ;

```

```

vbic_1(c,b,e,0) 'test' ;
tns_1(c,b,e,0) 'testm' ;
e_c(c,0) vc ;
e_b(b,1) vb ;
e_ac(1,0) sw(1,0) ;
e_e(e,0) ve ;
vc = 0 ;
vb = 0 ;
ve = 0 ;
end;
dc;
print: vbic_1, tns_1 ;
end; run;
dc(define);
c: forward gummel plot;
vb = an(0.4,1.2,40) ;
vc = vb ;
ve = 0 ;
print: i(vbic_1\c), i(vbic_1\b), i(vbic_1\c)/i(vbic_1\b),
      i(tns_1\c), i(tns_1\b), i(tns_1\c)/i(tns_1\b) ;
file: i(vbic_1\c), i(vbic_1\b), i(vbic_1\c)/i(vbic_1\b),
      i(tns_1\c), i(tns_1\b), i(tns_1\c)/i(tns_1\b) ;
end; run;
dc(define);
c: reverse gummel plot;
vb = an(0.4,1.2,40) ;
vc = 0;
ve = vb;
print: i(vbic_1\e), i(vbic_1\b), i(vbic_1\s), i(vbic_1\e)/i(vbic_1\b),
      i(tns_1\e), i(tns_1\b), i(vbic_1\s), i(tns_1\e)/i(tns_1\b) ;
file: i(vbic_1\e), i(vbic_1\b), -i(vbic_1\s), i(vbic_1\e)/i(vbic_1\b),
      i(tns_1\e), i(tns_1\b), -i(vbic_1\s), i(tns_1\e)/i(tns_1\b) ;
end; run;
ac(define);
c: forward fT;
f = 1.e6 ;
vb = as( 0.7, 1.0, 10.e-3 ) ;
vbc = 0.3, 0, -3 ;

```

```

vc = vb-vbc ;
print: f/imag(i(vbic_1\b)/i(vbic_1\c)), f/imag(i(tns_1\b)/i(tns_1\c));
file: f/imag(i(vbic_1\b)/i(vbic_1\c)), f/imag(i(tns_1\b)/i(tns_1\c));
end; run;
ac(define);
c: reverse fT;
f = 1.e6 ;
vb = as( 0.6, 1.0, 20.e-3 ) ;
vbe = 0, -1;
vc = 0 ;
ve = vb-vbe ;
print: f/imag(i(vbic_1\b)/i(vbic_1\c)), f/imag(i(tns_1\b)/i(tns_1\c));
file: f/imag(i(vbic_1\b)/i(vbic_1\c)), f/imag(i(tns_1\b)/i(tns_1\c));
end; run;
circuit(define);
vbic_1(c ,b0,0,0) 'test' ;
vbic_2(c1,b1,0,0) 'test' ;
tns_1(c ,b2,0,0) 'testm' ;
tns_2(c1,b3,0,0) 'testm' ;
dv = 1.e-6 ;
e_c(c,0) vc ;
e_c1(c1,0) vc+dv ;
j_b0(0,b0) ib ;
j_b1(0,b1) ib ;
j_b2(0,b2) ib ;
j_b3(0,b3) ib ;
r_b0(0,b0) 1.E6 ;
r_b1(0,b1) 1.E6 ;
r_b2(0,b2) 1.E6 ;
r_b3(0,b3) 1.E6 ;
end;
dc(define);
vc = an(5,0,100) ;
ib = 1.E-6, 1.0E-5, 1.E-4;
veaf = i(vbic_1\c)*dv/(i(vbic_2\c)-i(vbic_1\c)) ;
veafm = i(tns_1\c)*dv/(i(tns_2\c)-i(tns_1\c)) ;
print: i(vbic_1\c), i(vbic_1\s), vn(b0), veaf, veafm ;
file: i(vbic_1\c), -i(vbic_1\s), vn(b0), veaf,
      i(tns_1\c) , -i(tns_1\s) , vn(b3), veafm;
end; run;
finish;

```

References

- [1] H.C. de Graaff and W.J. Kloosterman, "New Formulation of the Current and Charge Relations in Bipolar Transistor Modeling for CACD Purposes" IEEE Transaction on Electron devices. Vol ED-32 p 2415 1985.
- [2] G.M. Kull, L.W. Nagel, S Lee, P Lloyd, E.J. Prendergast, H. Dirks: A Unified Circuit Model for Bipolar Transistors Including Quasi-Saturation Effects. IEEE Transaction on Electron devices. Vol ED-32 No 6 June 1985.
- [3] H.C. de Graaff and W.J. Kloosterman, "Modeling of the Collector Epilayer of a Bipolar Transistor in the Mextram Model", IEEE Transaction on Electron devices. Vol ED-42 p 274 February 1995.
- [4] L.C.N. de Vreede "HF Silicon ICs for Wide-band Communication Systems" Ph.D. Thesis Delft University of Technology ISBN 90-9009594-2
- [5] H.C. de Graaff, W.J. Kloosterman "The Mextram Bipolar Transistor model, Level 503.2, June 1995." Natlab Unclassified report Nr 006/94.

Author W.J. Kloosterman

Title Comparison of Mextram and the Vbic95 bipolar transistor model

Distribution

Nat.Lab./PI

PRL

PL-NAP

LEP

PFL

CP&T

WB-5

Redhill, UK

Briarcliff Manor, USA

Limeil-Brévannes, France

Aachen, BRD

WAH